

## DESIGN AND ENGINEERING ASPECTS OF THE MAIN COMPONENTS FOR THE WENDELSTEIN VII-AS STELLARATOR EXPERIMENT

Reinhard MATHIS \* and Jörg SAPPER

*Max-Planck-Institut für Plasmaphysik (IPP) [Euratom association], D-8046 Garching b. München, Fed. Rep. Germany*

Submitted 19 June 1989; accepted 13 September 1989  
Handling Editor: P. Komarek

In this paper the design of the essential components of the newly constructed Wendelstein VII-AS stellarator experiment at Garching are described, and the first technical and experimental results are reported.

### 1. Introduction

Stellarators are an alternative line to tokamaks in the field of toroidal confinement systems for fusion machines. In contrast to tokamaks, they allow net-current-free plasma operation and are therefore inherently suitable for continuous performance in a reactor. During the development of fusion machines stellarators were characterised for a long time by their complex confinement coil configurations because of the additional helical winding system on the vacuum vessel. It was supposed that such a winding system could only be developed with inadequate expense to reactor size, and that a modular reactor design would be restricted by conditions adhering to the helical windings. In [1] it was shown that helical windings can be replaced by using nonplanar coils, which provide combination of poloidal and helical currents. When in 1982 the Wendelstein VII-A experimental stellarator at Garching was redesigned as an advanced version, such a modular coil system was used the first time for the confinement system in a larger machine. In the following, we describe the design of the essential components of the newly constructed Wendelstein VII-AS machine, and report on first technical and experimental results.

### 2. Magnetic confinement system of W VII-AS

#### 2.1. Design and construction of the magnetic confinement system

The confinement field of the Wendelstein VII-AS experiment at Garching is exclusively generated by a coil set of modular design, composed of 45 nonplanar coils (Modular Field, MF-coils). Ten additional planar toroidal field coils merely serve to ensure the experimental flexibility of the system. The entire coil set consists of 5 equal field periods, each containing 9 nonplanar and 2 planar coils (see fig. 4). One of the MF-coils in each field period is enlarged to provide extensive (tangential or near-tangential) access to the plasma (e.g. for plasma heating by neutral beam injection and for diagnostics). The remaining 8 MF-coils are pairwise identical, with the two coils of each pair being assembled in symmetric position to the vertical mid-plane of a module and rotated by  $180^\circ$  on the horizontal coil axis [2] (fig. 1).

The applied magnetic forces and thermal loads impose high stresses on the coils and their support system. This together with physical and electrical requirements leads to specific problems in the manufacture and construction of the normal conducting Cu-coils:

- The dominating circumference stresses (typical average of 100 MPa over the coil cross-section) dictate the use of cold-hardened copper conductors.
- The generation of heat inside the coils requires an internal water cooling system.

\* Now with Balzers AG, Fürstentum Liechtenstein.

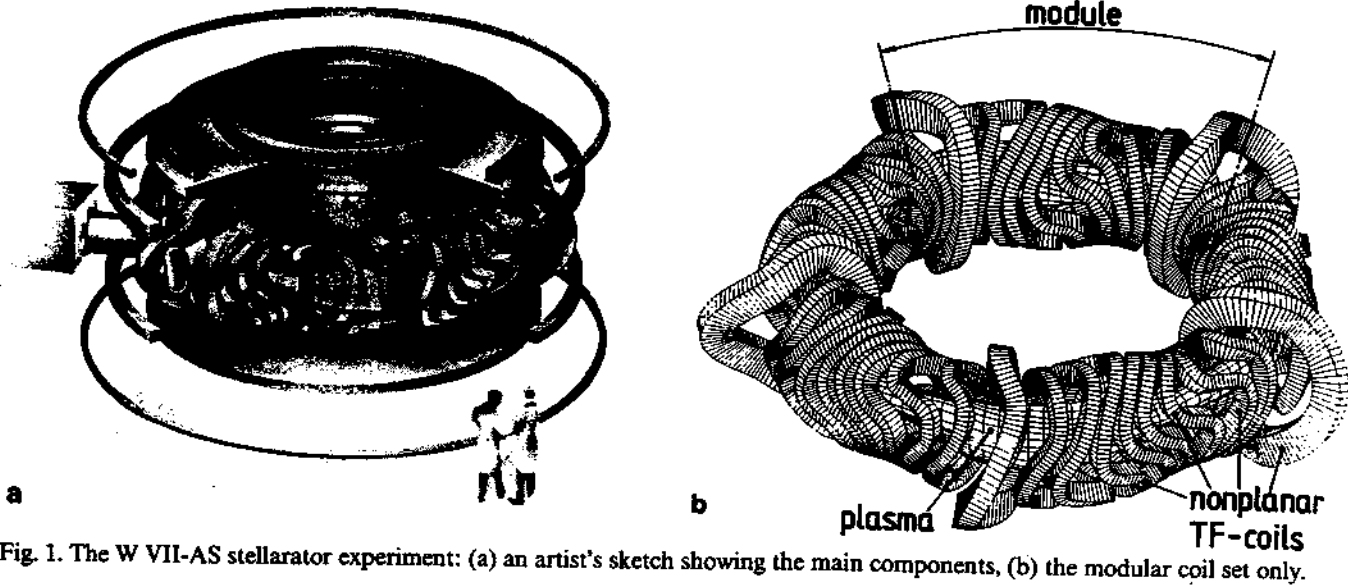


Fig. 1. The W VII-AS stellarator experiment: (a) an artist's sketch showing the main components, (b) the modular coil set only.

- The conductors must be three-dimensionally bent to radii of less than 0.1 m (minimum radius of curvature 0.08 m).
- For physical reasons the coil geometry must conform to strict tolerances. The error in the magnetic field principally has to be kept within a precision of  $10^{-3}$  or better, referred to the theoretical field calculated from exactly located currents in the coil areas. The most sensitive influence is caused by deviations in the geometric symmetric conditions within the modules and from coil to coil. These deviations destroy the good confinement properties of the field. Therefore a high reproducibility of geometries has to be achieved. Against this the absolute coil contour deviation re-

- ferred to a theoretical reference contour is of minor importance for a given machine because the wanted field configuration is not principally destroyed by a slightly altered coil set, yet the scientific goal of a machine might be depreciated if the field is modified significantly due to the contour deviations.
  - An electrically and, owing to the applied loads, also mechanically reliable insulation system is necessary.
  - The final mechanical and electric strengths of the coil have to be achieved by resin impregnation and curing in a high-precision mould.
- The forming of rigid high-strength conductors capable of withstanding the applied mechanical stresses would involve the difficulty of appreciable conductor

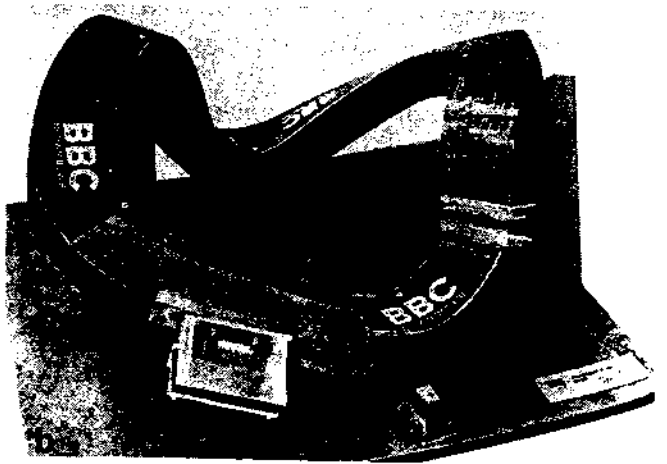
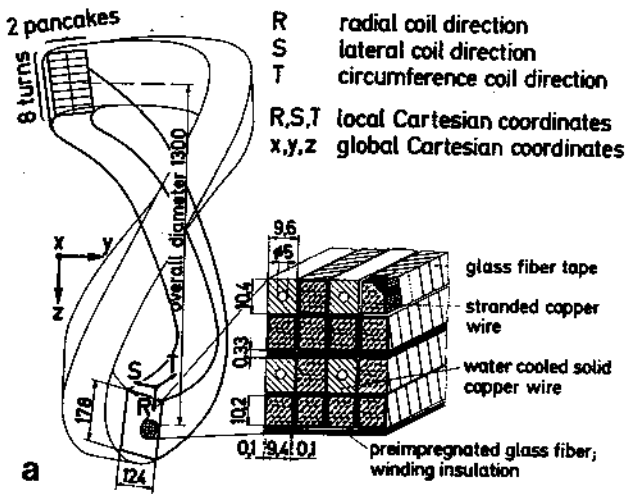


Fig. 2. Nonplanar MF-coils for W VII-AS: (a) coil concept composed of 2 pancakes and 16 copper turns separated by impregnated fibre-glass matting, (b) one field coil (number 1) before assembly.

“spring back” after coil forming and the possibility of insulation damage during coil forming (see, for example, [3]). To minimise these problems, the conductors are subdivided and each is built up from 160 single strain-hardened copper strands (0.8 mm in diameter each) joined together to a flexible, stranded copper wire and wrapped with glass-fiber tape. After extrusion (without using grease) the single copper strands are subsequently treated with an aliphatic polyamide primer (DZ80 from CIBA). This prevents oxidation and improves the adherence of the epoxy-resin to the wire surface. For cooling purposes solid, soft-annealed copper wires are added to the pack of stranded wires when they are wound into a mould to build up the coil. Oxides on the surfaces are removed by sandblasting and the primer painted on the surface. The inter-turn, pancake and surface insulation is provided by pre-impregnated high-strength glass-fibre tapes, composed of Silan-sized glass (fig. 2). Such an insulation system combines high dielectric strength and mechanical rigidity. To achieve mechanical rigidity, the coil is finally vacuum/pressure-impregnated with an epoxy resin system. The latter is a composition of Bisphenol A-type epoxy resin, MNA hardener and an accelerator. Before impregnation the conductor pack is pressed down to its final shape within the rigid mould [3]. After pre-drying, impregnation is carried out under vacuum, and finally the resin is polymerised (jellified and cured) [4].

The nominal magnet design parameters for the MF-coils are an operating time of 5 s equivalent rectangular current at full magnetic field – 3.0 T on plasma axis – with a duty cycle of 1 pulse every 180 s. The nominal coil current will be 592 kA and the copper cross-section is 14 640 mm<sup>2</sup>. For the enlarged MF-coil the coil current is 1 480 kA, and the copper cross-section 36 600 mm<sup>2</sup> (filling factor appr. 67.5% related to an outside coil cross-section of 100%). Ohmic losses during the duration of the pulse (mean terminal resistance 1.21 mΩ) lead to a temperature rise of the coolant water along the cooling path relative to the coolant inlet temperature.

In spite of the pulsed operation of the magnet the maximum temperature rise within the coil was calculated for steady-state conditions using a finite-element program and a simplified equivalent model. This calculation permits a conservative evaluation of the maximum temperature rise for each point along the wire and across its cross-section relative to the water inlet position. The measured temperature rise per duty cycle of the coil is, as expected, lower than that calculated [5].

To limit mechanical stresses the nonplanar coils must be sufficiently well supported against the magnetic forces but, nevertheless, allow some relative motion of the coils within this support structure. A system comprising the coil arrangement, the support elements and the support structures was therefore selected to build up the confinement magnet [6].

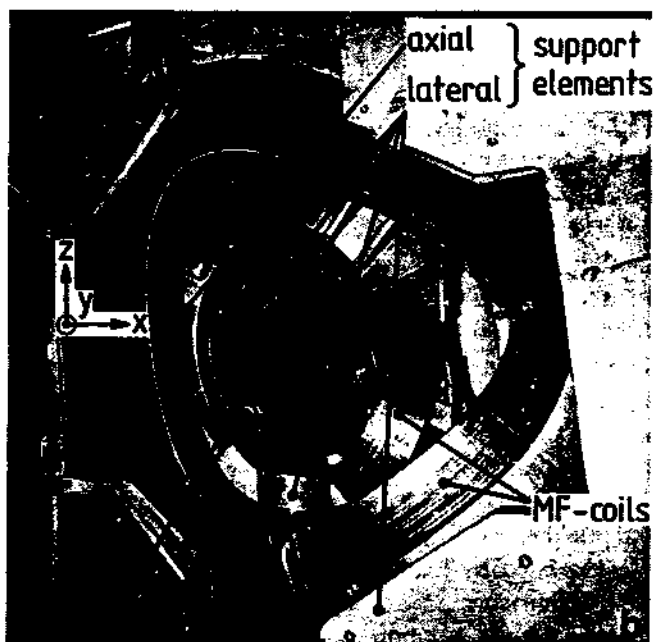
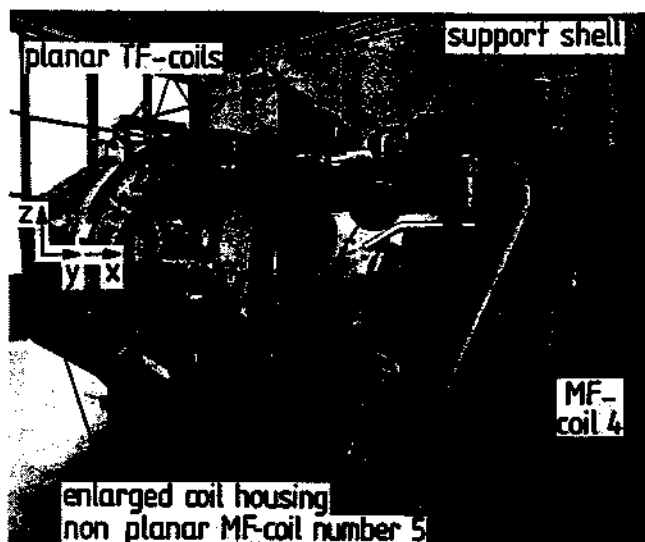


Fig. 3. An assembled module of the magnetic confinement system (only magnetic confinement system, vacuum vessel not installed): (a) seen from the outside, (b) view into one module.

The support structure for 8 of the nonplanar coils of one module is an external toroidal shell composed of two symmetric segments. It is a welded stainless-steel structure of 20 mm thickness (fig. 3a). Additional cast austenitic-steel support elements fix the lateral coil position (fig. 3b). Fiber slip coatings between the coil and the support elements considerably reduce friction if motion parallel to the surface occurs. The cast stainless-steel elements fixing the radial (R-direction) coil position are designed to support the coil on outside. This is done in the area determined by the sectional plane of the radial magnetic net force vector of one coil with the external shell, this force component being transmitted from the coil to the shell by pure pressure alone. All these structural members for one module are bolted together, forming the one part of the MF-coil support system. The second part of the system comprises single housings for each of the enlarged coils, these performing all of the functions already described (e.g. force transmission from the coil to the supporting structure (fig. 3).

Magnetically and thermally induced coil movements within these support systems are allowed in the radial and longitudinal coil directions and are prevented in the axial (lateral or toroidal) direction with respect to the coil plane. When the coil set is energised, the main magnetic force components are carried in different ways: the primary radial magnetic force is essentially carried by the cold-hardened copper conductor as (hoop) tension stress, while the lateral force component has to be transferred to the shell structure by support elements.

## 2.2. Stress analysis – Magnetic confinement system

The computational analysis of the structural mechanical behaviour for the W VII-AS MF-coils commenced by calculating the principal loads acting on the magnetic confinement system. The influence on displacements and stresses by the partially restrained coil movement described above is considered in the structural mechanical analysis, whereas (mutual inductance, electromagnetic fields and) magnetic volume forces for the single coils in the set arrangement are calculated in advance.

These calculations are done for critical magnetic force loading conditions occurring at a resulting magnetic field of 3.5 T on the plasma axis; an induction of 3 T is provided by loading the nonplanar MF-coils with their design current, and up to  $\pm 0.5$  T is provided in addition by the 10 additional planar TF-coils. The self and mutual inductances and electromagnetic forces for the coils were calculated with the EFFI (Electromag-

netic Field, Force and Inductance) 3D computer program [7]. The magnetic field distribution or  $B$ -vector field is computed by means of Ampere's law, and the magnetic pressure distribution by the vector cross product  $J \times B$ . Electromagnetic forces only act in the locally radial (R) and lateral (S) coil directions, whereas in the circumferential (T) direction (fig. 2a) no forces are induced owing to the electric current flow in this direction. These magnetic load calculations include the two principal components of the forces on these coils, coil self-forces on the individual coils and interactive forces between adjacent coils.

The basic model used for this electromagnetic calculation was the coil arrangement, the coils being represented as a series of connected, curved current density elements. The EFFI mesh discretisation depends on the mesh used for the structural mechanical analysis and will be shown later.

For mechanical reasons the coils must be allowed to expand in the radial and longitudinal directions by using antifricition coatings between the coils and support elements. Because thermally and magnetically induced movements in the lateral direction of these nonplanar coils are constrained, additional mechanical loads are applied. The influence of this load component on stresses and strains is considered in the structural mechanical calculation.

The most critical load combination for the magnetic confinement system appears at the end of the flat-top time (to be precise: at the onset of de-energization of the coil set), at which:

- the maximum magnetic forces are applied,
- the maximum temperature difference between the coils and the support system appears (a conservative value being 55 K),
- the maximum coil temperature (worst case  $80^\circ\text{C}$  → maximum temperature difference, maximum coolant temperature, steady-state conditions) with the lowest material strength values occurs.

If the expected safety margin at the end of this analysis were insufficient, the latter two temperatures and/or temperature differences would have to be restricted to less critical values.

First finite-element calculations using the SAP V code [8] together with material tests [9] demonstrated possible damage mechanisms (fatigue fracture or delamination of the copper wires and insulation system; permanent local deformation of the support structure). This knowledge served as a basis for a more detailed analysis using the MSC/NASTRAN code [10]. The inhomogeneous coil design leads to highly anisotropic and heterogeneous structural behaviour of this com-

posite system. For economic and numerical reasons, however, it is not possible to perform a 3D stress analysis giving separate consideration to each constituent of the coil. Instead, this system is replaced by an equivalent homogeneous orthotropic solid, whose material properties were calculated and/or measured (see Section 2.3). The overall material properties are described by nine engineering constants. Finally, the stress components for the constituent materials must be evaluated with due consideration of mechanical equilibrium and compatibility.

Three basic types of MSC/NASTRAN [10] finite-element structural models were used [11]. In a first model critical components of the coil support system had been selected. These results served as a basis for a detailed model of the most endangered component in this compound, the nonplanar coils. Special attention is directed to the coil with minimum radius of compound curvature (8 cm), which was found to be the modular field coil number 3 [12]. In a last step, this model is considerably refined in order to generate detailed stress tensors for those critical coil areas selected by comparing the results obtained from the FE analysis with the material behaviour of the coils.

If numerically possible, the geometry of the NASTRAN finite-element mesh for the coils or the coil cutout coincides with the EFFI current density element discretisation. This facilitates the transformation of the magnetic body forces (calculated with the EFFI code) to the kinematically equivalent nodal force components (volume forces) necessary as input data for the structural finite-element analysis.

### 2.2.1. Initial FE analysis

The initial model for the linear elastic FEM calculations was a 1/10 section of the assembly of all MF coils and their support system.

Restriction to such a reduced model is possible by utilising the given modularity of 5 and taking advantage of the geometry and magnetic load symmetries of the W VII-AS test device within one module. Gravity loads disturbing these load symmetries are negligible with respect to the magnetic loads. The enlarged coil, located in a single housing, is treated separately.

To generate the force data, an EFFI single-filament model representing each coil by 48 rectangular general current density elements (GCEs) was used (fig. 4). The coil geometry is described by the coordinates of the 4 coil edges at the boundaries of the GCEs. The NASTRAN mesh is achieved with different types of elements. The 4 nonplanar coils are meshed with 48 isoparametric 20-node solid hexahedron elements used

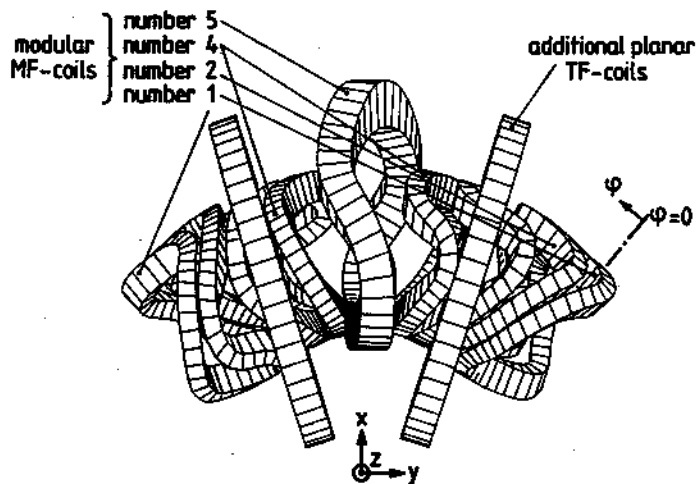


Fig. 4. Subdivision of one modular coil set into GCEs for the initial electromagnetic calculations.

for each coil (6912 d.o.f); for the support shell 653 quadrangular 8-node and 62 triangular 6-node plane-shell elements are used (11975 d.o.f); 298 hexahedron and 22 pentahedron solid isoparametric elements are used to model the support elements (6858 d.o.f); (e.g. figs. 5b, 5c and 6b for the FE subdivision).

The antifrictional coatings between the coils and their support elements in reality only allow the transmission of compressive (and shear, if  $\mu \neq 0$ ) forces, but not of tension force components perpendicular to the sliding surface. On the contrary, after the first computer run tension forces appeared in the calculations between these two components. Thus, in a second run all activated rigid-body connections exhibiting tension force components (132 out of originally 512) are disconnected. After this second run only small tension force components appeared at very few coil lateral surface FE nodes. In the deformation plots no undue intersections of the coils and their support elements are detectable. No further calculation run was therefore necessary.

With this initial analysis it was primarily the mechanical behaviour of the external support structures that was examined. For these components (manufactured from isotropic material) we calculated the equivalent (Von Mises) stresses (fig. 5). It was then compared with  $S_m$ , the safe stress at room temperature for the materials used. The calculated equivalent stresses for the support elements as well as for the support structure are lower than  $S_m$ . For these parts of the magnetic confinement system the results obtained show that the stresses are acceptable.

Maximum equivalent stresses were analysed for the nonplanar coils with peak values of up to only 100 MPa (fig. 5). Nevertheless, the decision whether this stress is

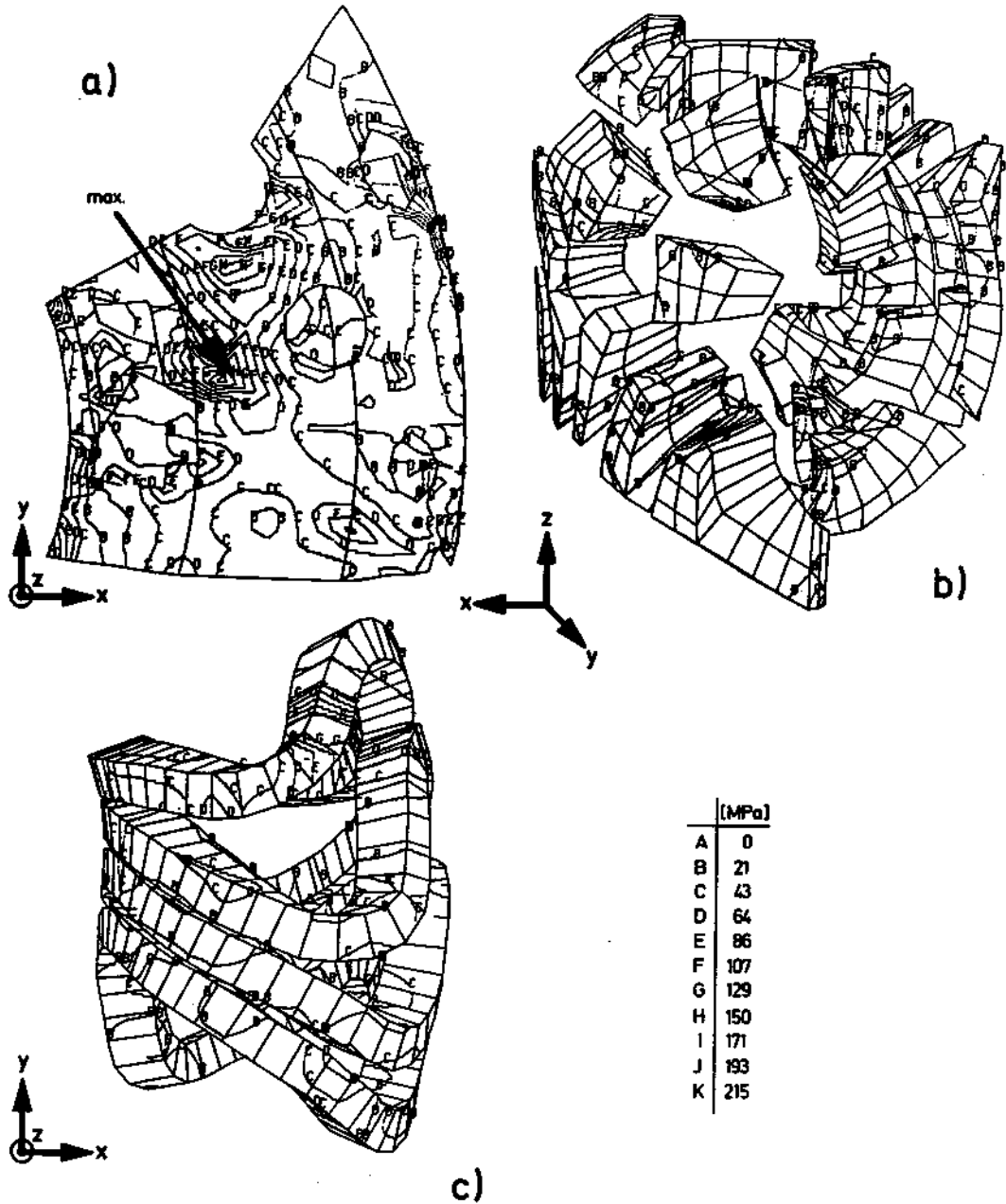


Fig. 5. Von Mises stresses from the initial stress analysis (1/10 section of the magnetic confinement system; isoequivalent stress contour plots): (a) support shell, (b) supporting structure, (c) nonplanar coil array.

admissible or not requires special attention due to the heterogeneous coil design with direction-dependent permissible stress values.

The maximum deflection of 1.17 mm for the support system occurs at the external shell (fig. 6).

### 2.2.2. Detailed FE analysis

In order to analyse more exactly the mechanical behaviour of the coils, each of the 5 geometrically different nonplanar coils was separately treated. Also

included in the first FE models were all adjoining support elements [8,9,11]. As expected, the maximum critical stress components (primary shear and hoop stresses) occurred in the coil with minimum radius of curvature (8 cm) – viz. coil number 3 – and vice versa [11,12]. All investigations were thus focused on coil 3.

The electromagnetic force calculations were done with an EFFI multifilament model representing the analysed coil by 768 rectangular GCEs. The other 54 coils – 44 nonplanar and 10 planar – of the experimen-

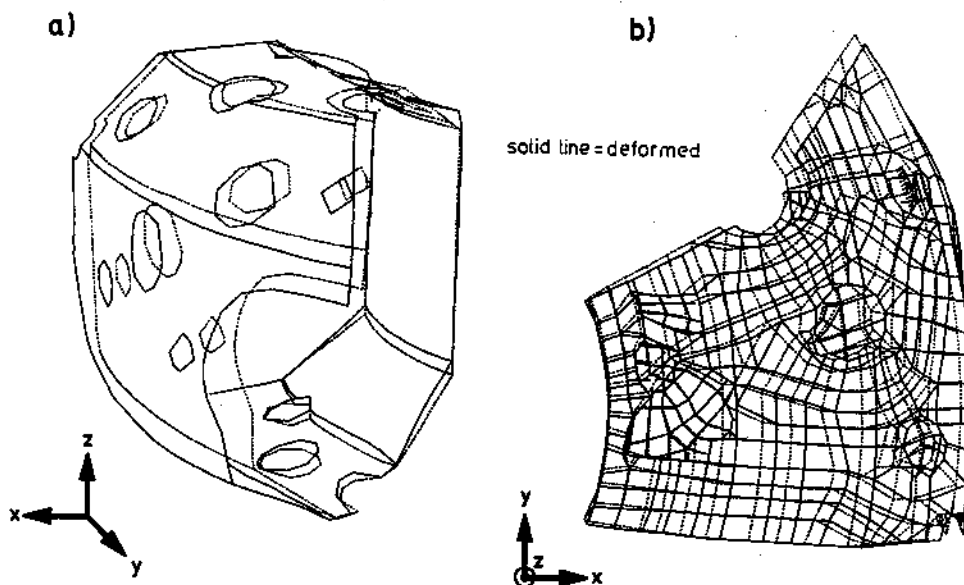


Fig. 6. Deflected and undeflected forms of a 1/10 section of the support shell (scaling factor = 100), initial stress analysis: (a) seen from outside the machine, only body edges considered, (b) top view, FE structural model.

tal device are less finely subdivided for economic (calculation time and available storage) reasons. Coil 3 is divided along its perimeter, into 96 sections or groups of GCEs (GGCEs), each section including 8 subcoils (2 by 4).

For the MSC/NASTRAN analysis the coil is idealised by means of 768 3D isoparametric 8-node solid hexahedron elements, the same subdivision being used as for the EFF1 mesh. The adjoining support elements are idealised by 702 elements of the same type as used for the coil (fig. 7). To realise free coil movement between the lateral support elements and the coil for the calculations, there are in the interface two separate FE nodes for the two components, connected by multipoint

constrains [10]. Frictionless coil movement is realised by coupling just the two translational degrees of freedom normal to the interfaces. The whole model is thus built up from 3321 nodes. The kinematic support of the selected cutout (coil with adjoining support elements) was achieved by fixing the support elements in the connecting areas to the external support shell. A linear elastic analysis is made for a homogeneous solid with anisotropic material behaviour for the coil (isotropic for the support structure). Owing to the coil design (fig. 2a), the axes of anisotropy follow the edges of the coil and the edges of the normal cross-section.

The maximum deflection calculated is 2.8 mm and occurs at the coil in an area radially outside the W VII-AS device, of which 1.2 mm is due to thermal expansion (the rest being induced by the magnetic loads). The deflection on the inside of the device is negligible (fig. 8). This is because the magnetic force distribution results in a net force component towards the torus axis, thus pushing the coils against the very stiff support elements positioned inside which fix the radial coil position, and a second component which stresses the coil similar to a vessel under inside pressure.

As represented in the next section, the failure behavior of such a compound in a multiaxial stress field may be best described by separately considering the two main constituents of the coil, the copper wires and the insulation system. Only selected stress components of the analysed stress tensor will essentially contribute to the failure of these constituents. The impregnated copper wires are thus mainly endangered by circumference

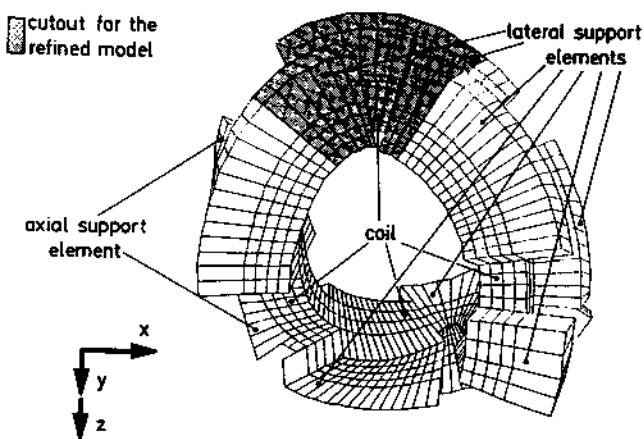


Fig. 7. FE structural model for the detailed stress analysis of modular field coil 3, including the adjoining support elements.

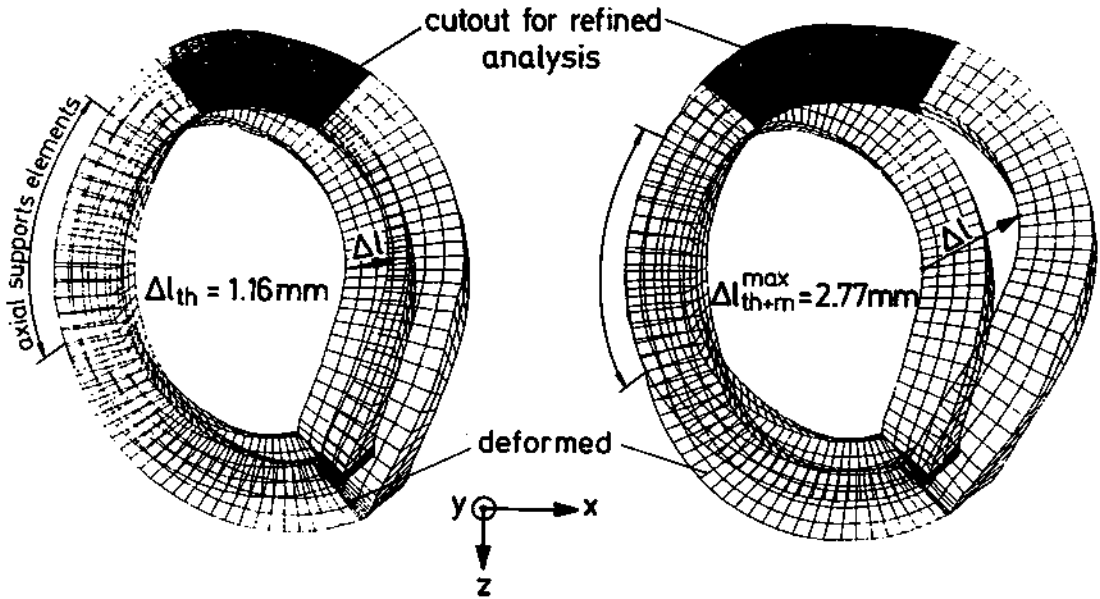


Fig. 8. Deflected and undeflected forms of modular field coil 3 (scaling factor = 100), detailed stress analysis: (a) deflection induced by thermal expansion, (b) superposed thermal and magnetic deflection.

( $\sigma_T$ ) and shear ( $\tau_{R,T}$ ;  $\tau_{S,T}$ ) stresses, the insulation system by out-of-plane direct ( $\sigma_T$  or  $\sigma_S$ ) and in-plane shear ( $\tau_{R,T}$  and  $\tau_{R,S}$  or  $\tau_{S,T}$  and  $\tau_{S,R}$  respectively) stresses (for further details see Section 2.3 and [8,9,11,12,13,14]). On this basis, critical stress combination for these two constituents are selected from the FE analysis.

Comparison of these results with measured material strength values showed that two critical stress combinations endangering the impregnated stranded copper wires occurred:

- Superposed on the maximum hoop stress of  $\sigma_T = 105$  MPa (applied to the whole coil cross-section) is a shear stress component of 12 MPa. The failure criterion with such a biaxial stress field (a first approximation) would be yielding of the copper wires; measurements distinctly indicated higher values for the yield strength – even on the assumption that only the copper wires will carry the hoop stresses (copper volume filling factor is  $\geq 0.63$ ).
- Superposed on the maximum shear stress of  $\tau_{ST} = 55$  MPa in the copper wires is a direct stress component of  $\sigma_T = 50$  MPa in the wire direction. The failure criterion here would be delamination in the impregnated copper wires. From the mechanical tests carried out it can be deduced that this load combination is more critical.

Based on adequate conclusions critical stress combinations for the insulation system and/or the adhesive interface plane are as follows:

- maximum in-plane shear stress of  $\tau_{ST} = 55$  MPa with superposed out-of-plane direct (tension) stress of  $\sigma_S = 13$  MPa,
- maximum out-of-plane tension stress of  $\sigma_R = 20$  MPa with superposed in-plane shear stress of 18.5 MPa (resulting from  $\tau_{R,T}$  and  $\tau_{S,R}$ ),
- in-plane shear stress of 26 MPa with superposed out-of-plane tension stress of 10 MPa. The failure criterion for all three stress combinations would be delamination in the insulation system or adhesive/cohesive breakdown of the insulation/copper wire bond face. When comparing these results with measured strength values, one can conclude that all 3 cases are critical.

All critical stress combinations in the insulation system as well as the most critical for the copper wires are located in or around the coil area with maximum curvature. The accuracy of the calculated stresses can be estimated by, for example, checking the stress distribution at free surfaces and edges. It is then readily seen that the idealisation accuracy is not sufficient. Further mesh refinement is therefore necessary.

### 2.2.3. Refined FE analysis

The last step in the successive mesh refinement was to idealise the mechanically most endangered part of the coil separately. This selected cutout of the coil contains a strongly curved part of MF-coil 3 and will allow more detailed classification of the strain conditions.



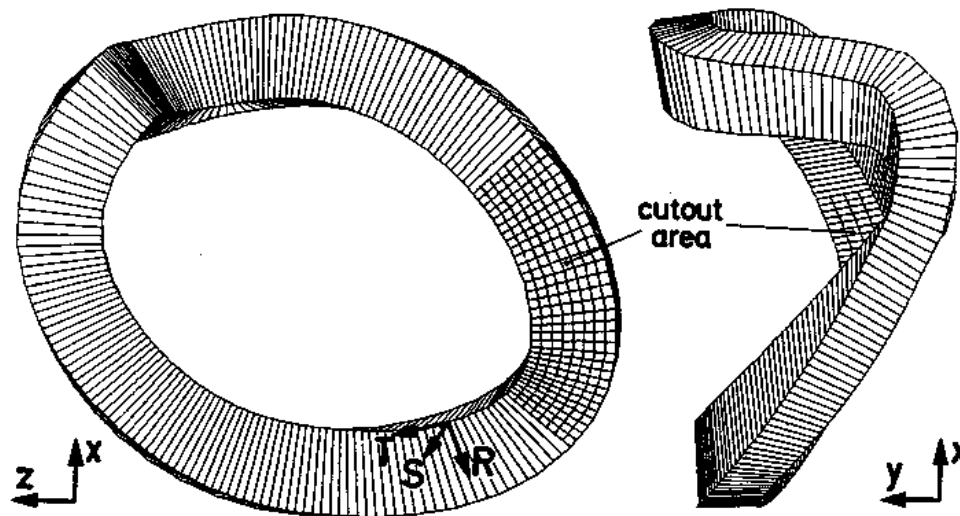


Fig. 9. Subdivision of modular field coil 3 into GCEs and GGCEs for the refined electromagnetic calculations.

The refined EFFI multi-filament model for the selected cutout contains along its perimeter 18 sections (114 for the whole coil; for the cutout each GGCE of the detailed FE analysis is divided into 2 new GGCEs), each section of the cutout including 60 subcoils (6 by 10). The rest of these coils and, as before, all adjoining coils are coarse-meshed (fig. 9). Because of the comparatively steep gradient in the magnetic volume loads in the coil cross-section – in contrast to the coil circumference direction – the mesh subdivision in the latter direction is less fine. The kinematically equivalent nodal force components at the NASTRAN nodes were computed by interpolating the body force values at the EFFI mesh (by BQUIN [15]).

The mesh for the structural analysis is achieved with the same element type as for the detailed FE analysis. The coil circumference direction is now meshed by 60 elements; in the coil circumference direction the cutout is subdivided into 30 sections (1800 elements). The mesh of the adjoining support structure (440 elements) coincides at the contact faces with the coil mesh. Includes is now an elastic bed – meshed by 400 elements – built up from a glass/epoxy-resin composite and arranged between the coil and the support structure. The boundary conditions at the end sections of the cutout were derived from the detailed FE analysis, care being taken that the results from the latter were put in as prescribed displacements. All other boundary condi-

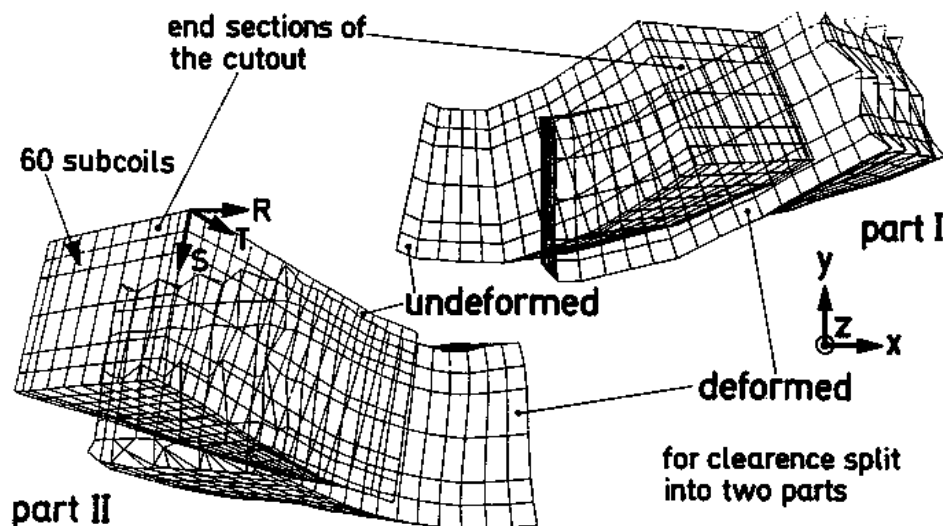


Fig. 10. Deflected and undeflected forms of the cutout of modular field coil 3 (scaling factor 10), refined stress analysis.

tions (e.g. realizing the coil movement; support conditions; material behaviour; two computer runs for realising force transmission from the coil to the support structure by compression loads only) are as before. The whole structure consists of 3 763 grid points.

For the new calculations the resulting displacements from the coarse analysis are prescribed only at the grid points of the first analysis; no interpolation for the displacement tensor for any of the other nodes was carried out (fig. 10). All results at the end sections of the cutout are thus inaccurate; the influence of this simplification outside the end sections of the cutout is negligible.

The displacements calculated with the refined model are comparable to those obtained with the coarse model.

The critical stress combinations were selected on the same basis as described for the detailed analysis. For the impregnated, stranded copper wires the results obtained are not much different from those of the previous analysis (limited of course to the coil cutout): Superposed on the maximum hoop stress of  $\sigma_T = 92$  MPa in the copper wire (all values applied to the whole coil cross-section) is a shear stress component of  $\tau_{R,T} = 20$  MPa (previous analysis in the same area:  $\sigma_T = 70$  MPa/ $\tau_{R,T} = 16$  MPa). Superposed on the maximum

shear stress in the copper wire of  $\tau_{S,T} = 39$  MPa is a hoop stress of  $\sigma_T = 37$  MPa (previously  $\tau_{S,T} = 55$  MPa,  $\sigma_T = 52$  MPa).

From many material tests and a prototype coil test (see Section 2.3 and [5,9,11,12,13,14,16]) no risk of fracture or delamination in the impregnated, stranded copper wires, even under fatigue loads is seen.

All critical stress combinations for the insulation system/interface planes detected from the detailed analysis are concentrated on the selected cutout. In this refined analysis these combinations are as follows:

- Maximum in-plane shear stress  $\tau_{T,S} = 39$  MPa ( $\tau_{R,S} \approx 0$ ) with superposed out-of-plane tension stress of  $\sigma_R = 15$  MPa;
- Maximum out-of-plane direct tension stress of  $\sigma_R = 20$  MPa with superposed in-plane shear stresses of  $\tau_{R,T} = 16$  MPa;
- out-of-plane direct compressive stresses in the analysed order of magnitude (up to 90 MPa, negligible shear) considerably reduce the risk of interface damage and delamination if in-plane shear stresses act simultaneously; the maximum combination of out-of-plane direct stress  $\sigma_S = 60$  MPa and superposed in-plane shear stress  $\tau_{S,T} = 20$  MPa will thus not cause damage to the insulation system.

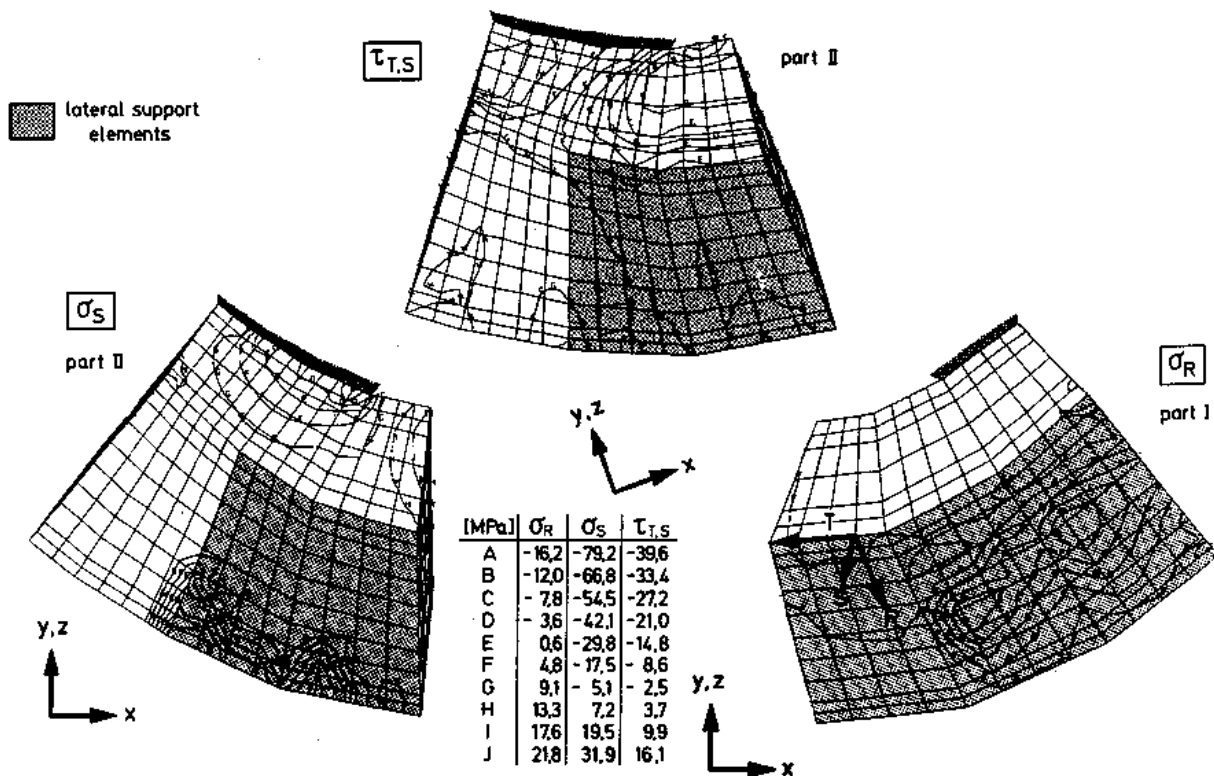


Fig. 11. Selected stress components from the refined stress analysis for the cutout of modular field coil 3 (isoequivalent stress contour plots).

Most critical is the first-listed load combination, occurring in T-R planes (so-called pancake insulation layers, see fig. 2a). Normal insulation systems would not be capable of withstanding this load combination, but the special design selected for these planes with special insulation materials used (prepreg layers; see [9,16]) will considerably raise the limiting range of stresses. For manufacturing reasons this reinforcement is not possible in T-S insulation planes with the maximum load listed in second place. Nevertheless, the insulation system chosen will withstand this maximum load combination occurring in the insulation planes (direct tension 20 MPa, shear stress 16 MPa) for the envisaged lifetime of the W VII-AS device,  $5 \times 10^4$  load cycles, at 80 °C.

One of the important problems in this analysis was to calculate very accurately the (comparatively small) stress components endangering the coil, whereas, for mechanical strength reasons, the dominant stress is not a limiting factor. But this is known to be difficult if displacement models are used. Especially for this refined analysis, it was found that boundary conditions, such as stress-free edges, disappearance of in-plane shear and out-of-plane direct stresses at free surfaces, or negative out-of-plane direct stresses and disappearance of in-plane shear stresses ( $\mu = 0$  postulated) at sliding surfaces, are very accurately satisfied (fig. 11).

### 2.3. Material tests – Magnets

The maximum calculated Von Mises stress for the support shell – a welded stainless-steel structure – was 190 MPa, localized to a very small area (fig. 5a). The yield strength limit, which for an austenitic steel in a first approximation is equal to the fatigue strength limit, for type 304 LN (German Standard 1.4311) is 270 MPa. Because the cast austenitic support elements are less stressed than the shell (fig. 5b), there should be no fracture risk for this structural member of the confinement system either. Both of these components are designed for minimum deformation.

The elastic bed and antifrictional coating between the support elements and the coil are primarily stressed by compressive loads. They rise to 90 MPa. Neither the function of the fibre slip coatings – low coefficient of friction – nor that of the elastic bed (8 mm thick on average) – large area adaption of the steel elements to the nonplanar coils, which could possibly be made worse by creep processes – should be influenced.

More complicated is the mechanical valuation of the nonplanar coils because of the heterogeneous coil design exhibiting orthotropic material behaviour. For clarity, in a first step the two main constituents of the coil, the

impregnated, stranded copper wires and the insulation system, are considered separately. Later on, the mutual interference of these two constituents is additionally investigated. Because strength values for this specific design of nonplanar coils are not available, an extensive test program for measuring material properties was carried out (see also [5,6,8,9,11,12,13,14,16]).

#### 2.3.1. Stranded copper wire

The mechanical strength tests started with the single copper strands of the stranded copper wire. The material used for these strands is Ag-alloyed OF-copper (OF-CuAg 0.1, German Standard DIN 1787/17666/40500), strain-hardened to a yield strength of  $\geq 230$  MPa. The silver content guarantees that there is no strength loss even under the final impregnation process at elevated temperature. The corresponding material tests were carried out after precipitation of the copper wires for 20 h at 150 ° and 1 h at 300 °C, and no strength reduction could be detected after this treatment. Complete and satisfactory priming of the strands was ensured by controlling the priming process (e.g. surface purity, extrusion velocity, primer bath viscosity, furnace temperature). The epoxy-resin used is described in Section 2.3.2.

The impregnated stranded copper wires are arranged within the coils in such a way as to be able to carry the dominating stress component occurring in such a construction unit, which is the hoop or tangential direct stress component. Besides this dominating stress component, there is also secondary an (external) shear stress  $\tau_{R,T}$  and  $\tau_{S,T}$  of up to 39 MPa endangering the nonplanar coils. Owing to the stranding angle of 10 ° of the single copper wires to the (tangential) T-direction and the inhomogeneous strand design (copper and epoxy-resin) the tangential direct stress component leads to micro-mechanical additional stress components of approximately  $\tau_{\text{internal}} \approx 0.17 \sigma_T$  occurring between single copper strands [9,14,17] which are superposed on the external shear stresses  $\tau_{S,T}$  and  $\tau_{R,T}$ .

In order to find out whether or not the copper wires are mechanically endangered by the given (calculated) stress combinations, static and dynamic material tests with individual, vacuum-pressure-impregnated, stranded copper wires were carried out. Possible damage mechanisms occurring under the given mechanical loads are yielding, fracture or fatigue fracture of the single copper strands and static or fatigue delamination between the single copper strands within the epoxy resin or at the epoxy/copper interface. The tangential direct stress component  $\sigma_T$  in the first case and the superposition of external and internal shear stresses in the second case

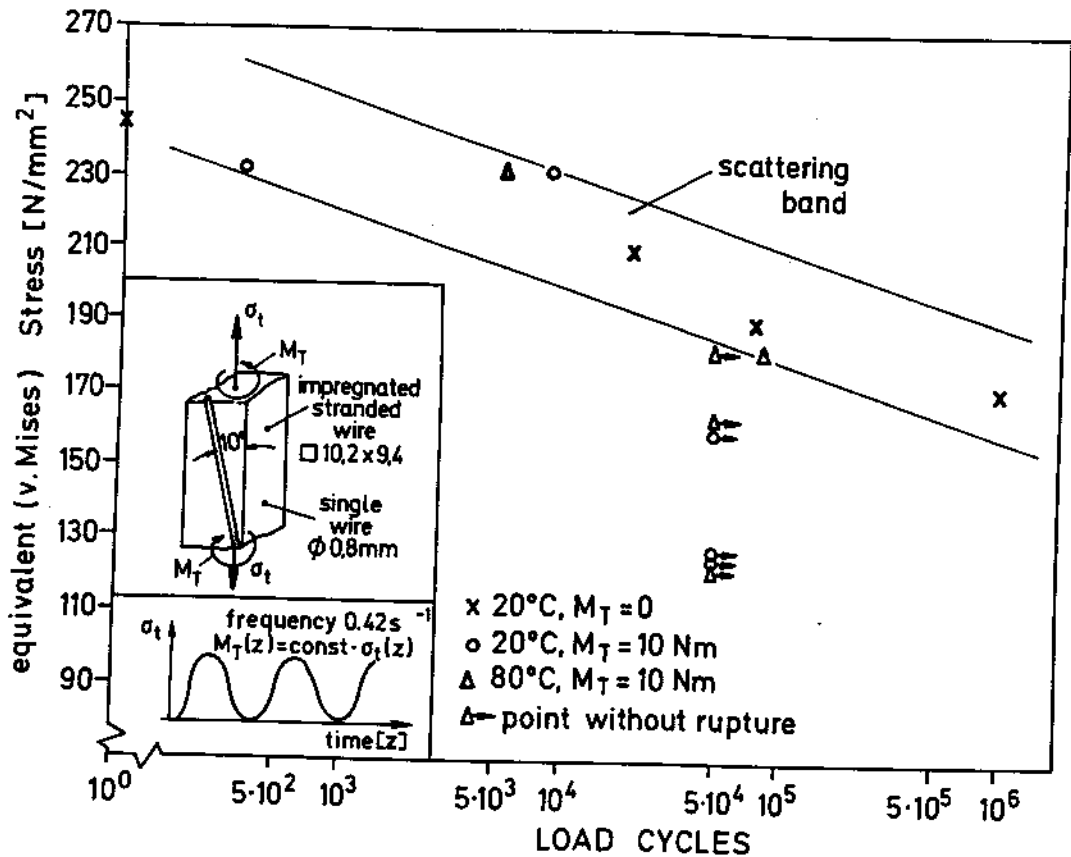


Fig. 12. Fatigue strength values under tension and combined tension-torsion loads for single-impregnated, stranded copper wires.

are the primary damage-inflicting loads. Static and dynamic tension and combined tension-torsion tests [9] were thus conducted (fig. 12).

The measured ultimate strength value in macroscopic pure static tension tests is 245 MPa, in pure fatigue tension tests at the envisaged lifetime of the test device ( $5 \times 10^4$  test cycles) appr. 190 MPa. The failure criterion is damage to the copper wires. Even under tension loads on which (external) torsional moments of 10 Nm are superposed, no delamination of the copper/resin interface or within the resin matrix occurs. The mechanical strength behaviour under these load combinations is essentially determined by the copper content. The results of the material tests are therefore summarised in a Wöhler Diagram, in which the maximum equivalent Von Mises stresses are plotted versus the load cycles (fig. 12). These equivalent stresses are calculated without taking into account the copper filling factor in the impregnated wire (app. 83%). The tests are carried out at 20°C (room temperature) and 80°C, the maximum temperature expected to occur in the nonplanar coils.

In this tension and combined tension/torsion fatigue tests the copper wires were undamaged after the

envisaged lifetime of the device ( $5 \times 10^4$  cycles) with Von Mises stress values  $\sigma_{VM} \leq 190 \text{ MPa}$ . There is no significant difference in the lifetime of samples when the test temperature is varied between 20° and 80°C, only the (dynamic) elongation and twisting amplitude are a little bit higher for the elevated temperatures. Contrary to this, the permanent twisting after the end of testing is at least 3 times as high at 80°C. This is due to the elevated creep rate of the epoxy resin at this temperature.

From the FE calculations described in Section 2.2 and elsewhere [11,12] a maximum resulting equivalent stress in the stranded wire of 100 MPa can be calculated from the analysed stress tensors. This maximum stress value occurs in nonplanar field coil number 2 at maximum magnetic field values and maximum temperature. The value also takes into account the additional shear resulting from tensile stresses in the stranded wire. The available safety factor for the maximum load combination and an envisaged lifetime of the W VII-AS test device ( $5 \times 10^4$  full load pulses) is  $\approx 1.9$ . The impregnated, stranded copper wires of the "compound" used in the coil should no be endangered under the given load combination.

2.3.2. Insulation system

The conventional vacuum-impregnated epoxy-glass insulation system chosen, Orlitherm OH 67-UM [19], is about the same as that used for the JET poloidal coils [20,21]. A primer is used to improve the adhesion of the resin matrix to the copper. The dielectric rigidity of the insulation system is ensured by the use of Silan-sized glass (pre-impregnated for use as insulation layers, dry glass tapes used to wrap the stranded wires). For such an insulation system the most critical stresses are in-plane shear (of the insulation layer) and out-of-plane direct tensional stresses or a combination of both. A special type of specimen (Type E, fig. 13), subjected to the same manufacturing processes as the nonplanar fields coils of W VII-AS has been developed.

First of all, these tests are useful for identifying strength-limiting components of all possible insulation/wire combinations of the insulation system. The result also serves to establish mechanical strength values. Tests have been carried out (see also [9,14]), using: (a) stranded wires only and dry glass; (b) solid wires only and dry glass; (c) stranded wires with one solid wire in the push-out position and dry glass; (d) stranded wires only and prepreg layers in selected positions; (e) stranded wires with one solid wire in the push-out position and prepreg layers in selected positions. The primer hardening conditions, the resin system combination as well as

the impregnation and hardening conditions were identical in all 5 cases. In static tests the fracture load was first reached in samples built up from stranded copper wires only, wrapped with dry glass [9]. All other possible combinations – with solid wires and/or prepreg layers – show better mechanical resistance, with strength values up to 25% higher than the critical value. All further investigations were thus focused on these mechanically limiting wire/epoxy/glass combinations.

One of the problems of these E-type specimens (fig. 13) is the nonlinear shape of the in-plane shear and the additional appearance of out-of-plane direct stresses [13,14]. Thus, it is not readily possible to select the critical, failure-releasing stress combination.

Similar difficulties occur with B-, C- and D-type specimens [9,13,14,20] (fig. 13). The stress distribution for E-type specimens were calculated using finite elements, the results for the two most important stress components being shown in a simplified graph in fig. 14; for further information see [13,14].  $\bar{\tau}$  is the average shear stress, calculated from the applied load divided by the shear surface ( $4 \times$  the lateral surface of a stranded wire). Optimisation of the flexibiliser content and of the curing and hardening conditions of the resin as well as the use of accordingly tuned glass tapes improved the available fatigue strength of the insulation system for the envisaged lifetime of the device ( $5 \times 10^4$  load cycles)


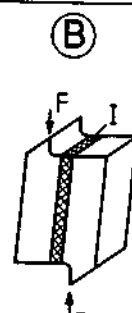
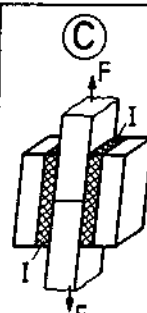
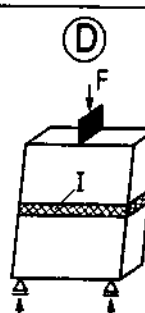
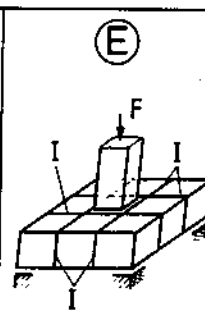
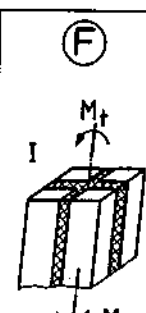
specimen type						
main insulation stress	tension	shear	shear	shear/pressure	shear	shear
main acting stresses	—	shear stress gradient in load- (insulation-) direction		add. out-of-plane pressure stresses	add. out-of-plane tension or compression stresses	shear stress gradient in cross section
wire type	not possible with stranded wires				for stranded wires	
references	Koch/Maix/ Nylund, Last/Bond/ Salpietro;	Koch/Maix/ Nylund, Rauch/König/ Schmid, Last/Bond/ Salpietro;	Rauch/König/ Schmid, Last/Bond/ Salpietro;	Koch/Maix/ Nylund, Rauch/König/ Schmid, Last/Bond/ Salpietro;	Mathis/Mukherjee/ Sapper, Buck/Klee/Mathis, Buck/Osen/ Bodisco/Winkler;	Buck/Klee/ Mathis, Buck/Osen/ Bodisco/ Winkler;

Fig. 13. Different types of small test specimens (copper-insulation compound) used for measuring insulation strength values.

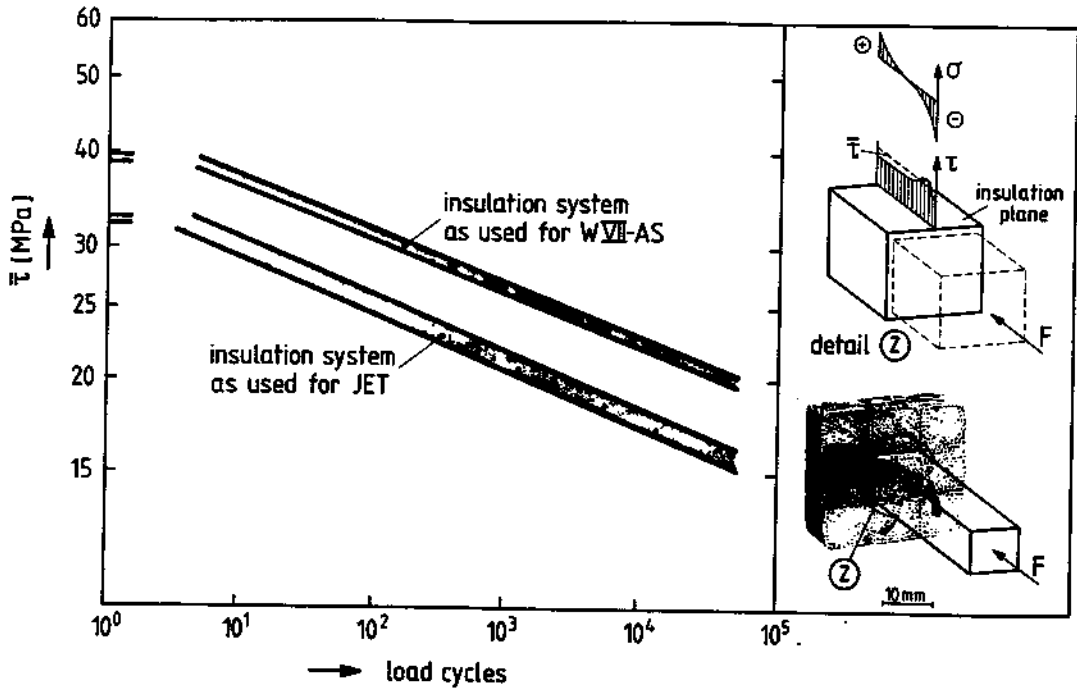


Fig. 14. Measured fatigue shear strength for two different types of insulation systems, ejection type test arrangement ( $80^{\circ}\text{C}$ , principal stress ratio  $R = 0$ , frequency  $0.25\text{ s}^{-1}$ ).

by appr. 30% (fig. 14). Test conditions such as temperature, frequency and so on have a decisive influence on the fatigue strength. For tests carried out using an F-type specimen, the optimised insulation system was found to have an endurable shear time strength after  $5 \times 10^4$  load cycles of 20 MPa at  $80^{\circ}\text{C}$  (for the shear stress distribution in this orthotropic compound torsion bar see [9,13,14]). Transferring these measured results to the coils is difficult because of some specimen-specific properties (e.g. occurrence of the shear stress peak at the surface – for the impregnation process different shrinkage conditions and different creep behaviour – or

the shear gradient in the specimen cross-section – reduction of peak stresses by creep). Deducing a reliable strength value for such an insulation system in an approximately biaxial stress field is complicated by such specimen-specific shortcomings, e.g. in the shear stress distribution, in specimen preparation or through edge effects. This is reliable for all specimens given in fig. 13.

The results obtained from E- and F-type specimen tests can be transferred to a shear-/direct-stress time strength diagram. On the same basis – namely  $5 \times 10^4$  load cycles, stranded copper wire with dry glass, resin as used for JET – additional strength values may be estimated from the measured values [9,14,16,19,20,21], converted with the knowledge resulting from E-type specimen tests (see [13,14] and fig. 13).

A range of safe working conditions in such a stress field may be defined on the basis of all these results (fig. 15). Similar considerations are possible for the optimised insulation system; for clarity, fig. 15 contains only measured values. The range of uncertainty for endurable strength values is wide. This is intensified by the problem of applying these values obtained from laboratory samples to the coil. The determined strength value with the uncertainty range is very close to analysed stress combinations in the coil. Further investigations are thus necessary for defining safe working conditions for the insulation system of the nonplanar coils.

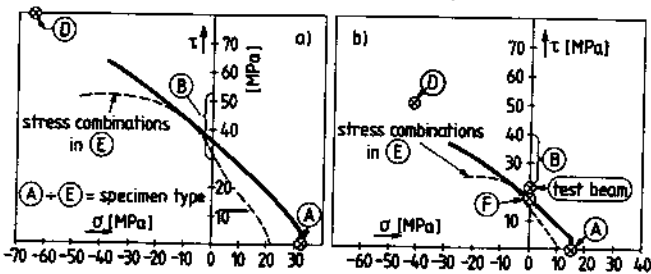


Fig. 15. Strength results obtained from different specimen types and deduced lowest damage limiting curve, shown in a biaxial strength field for "JET resin": (a) static loads,  $80^{\circ}\text{C}$ ; (b) fatigue limit,  $5 \times 10^4$  load cycles,  $80^{\circ}\text{C}$ , principal stress ratio  $R = 0$ , frequency  $\approx 0.25\text{ s}^{-1}$ .

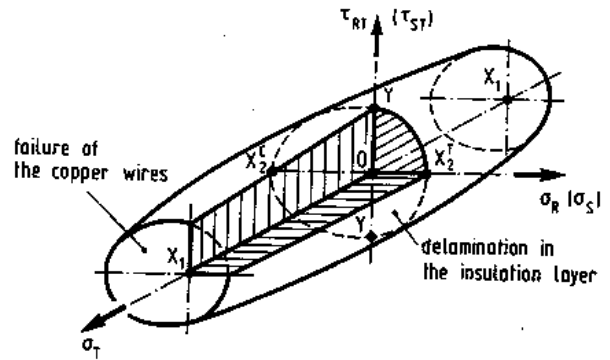
2.3.3. Beam and prototype coils tests

Three straight models (beams) of exactly the same internal construction as the original coil with the original coil cross-section were made for material tests. They served for measuring the overall material properties of the inhomogeneous, orthotropic material as well as for measuring material strength values.

One model was first tested under pure static bending to measure Young's modulus in the coil circumference direction – the most important of the three E-moduli. In a second test these beams were subjected to torsion in order to analyse shear moduli, in which shear isotropy with reference to the shear moduli in the cross-sectional plane of the coil  $G_{RT} = G_{ST}$  is given [9]. These measurements [9,14,18] together with small sample tests [5,9,14,18] and analytical calculations [9,13,14] serve to determine the nine engineering constants necessary to describe the mechanical behaviour of the homogeneous orthotropic equivalent system.

For mechanical fatigue tests the beams were loaded in a special test device – an eccentrically supported bending beam, fitted with freely moving and twisting end sections [9,14]. This combined bending and torsion leads to stress combinations similar to those analysed for the nonplanar coils; see Section 2.2. The test temperature was 80 °C – the maximum working temperature of the magnet coils – and the test frequency 0.25 Hz (sinusoidal). The results of these tests are summarised in table 1 and fig. 15.

As expected after the laboratory tests there was no failure of the copper wires, either fracture of single wires or delamination within the stranded wires. The damage mechanism under the selected load combinations (test beam II and III) was delamination in the “insulation layer” between single wires [5,9,14,16]. Within the winding insulation, which is composed of



$$\frac{\sigma_T^2}{X_1^2} + \frac{\sigma_{R(S)}^2}{X_2^T \cdot X_2^C} + \frac{\tau_{RT(ST)}^2}{Y^2} - \frac{\sigma_T \cdot \sigma_{R(S)}}{X_1 \cdot \sqrt{X_2^T \cdot X_2^C}} + \frac{X_2^C - X_2^T}{X_2^T \cdot X_2^C} \cdot \sigma_{R(S)} \leq 1$$

- $X_1$  fatigue strength for copper
- $X_2^T$  fatigue tensile strength perpendicular to conductor direction (out-of-plane direct strength of the insulation system)
- $X_2^C$  fatigue compressive strength perpendicular to conductor direction
- $Y$  fatigue in-plane shear strength in the insulation layer or in the impregnated conductor

Fig. 16. Approximate failure surface for the modular field coils.

prepreg layers, no delamination could be detected at the onset of failure start. This corresponds to the results described in Section 2.3.2. The beams had been produced by normal coil manufacturing techniques, but with “JET resin” (see Section 2.3.2) and component glass tapes in the impregnation process. The most important results of these beam tests may be summarised as follows:

- The mechanically limiting constituent in the coil is the insulation system.
- For the impregnated, stranded copper wire there is no danger of fracture or delamination under the expected stress combinations.
- For the optimized insulation system the admissible in-plane shear stress in the insulation should be approx. 30% higher, according to the results, described in 2.3.2. Thus the admissible in-plane shear stress for  $5 \times 10^4$  full-load test cycles at 80 °C for a test beam with optimized resin system is expected to be also 30% higher than the values obtained from the original beams (see table 1).
- The fracture behaviour of this compound material is very goodnature. After the first indications of delamination were detected, it took a long time (additional load cycles) for fracture propagation to occur; a total failure in the mechanical sense did not

Table 1  
Results of combined tension/compression-torsion fatigue tests with straight test beams having original coil cross-section (80 °C, principal stress ratio  $R = 0$ , frequency  $\approx 0.25 \text{ s}^{-1}$ )

	test number			test arrangement
	I	II	III	
$\tau_{max}$ [MPa]	16	28	22	
$\sigma_{max}$ [MPa]	150	150	103	
$n_{delamination}$	$> 5 \cdot 10^4$	$\approx 10^3$	$\approx 10^4$ *	

\* initial loading (static): = 60% above dyn. load

occur (only increasing plastic deformation coupled with propagating delamination in the insulation layers).

From all these material tests it can be concluded that the failure behaviour of such a compound can be reasonably well described by the Tsai-Wu criterion [22,23,24,25], originally derived for unidirectionally reinforced composites in a biaxial stress field (fig. 16). For the expected different local combinations of stress components this strength hypothesis is based on the fact that the coil or the two main constituents of the coil will be mechanically endangered only by selected stress combinations. The impregnated copper wires are thus subjected primarily to hoop or circumference stresses  $\sigma_T$  and secondarily to the shear stress components  $\tau_{R,T}$ ,  $\tau_{S,T}$ . Other stress components of the local stress tensor are negligible. On the other hand, the glass/epoxy-resin insulation system and the insulation/copper adhesive interface are subjected primarily to direct stress acting in the insulation (interface) planes. In-plane direct and out-of-plane shear stress components are secondary effects.

For the envisaged lifetime of the test device ( $5 \times 10^4$  full load pulses) at maximum working temperature of the coils the fatigue strength limits are as follows (for optimised insulation systems):  $X_1 > 150$  MPa (reference coil cross-section);  $XT_2 \approx 21$  MPa;  $|XC_2| > 55$  MPa;  $Y \approx 27$  MPa (see fig. 16). On this basis, critical stress combinations are selected from the results obtained from the FE-analysis described in Section 2.2 and [10,11].

The maximum calculated hoop stress of  $\sigma_T = 105$  MPa, on which a shear stress component of 12 MPa is superposed, appears in the detailed analysis of Section 2.2. These values are applied to the whole coil cross-section in accordance with fig. 2a, and they can be transformed to the impregnated and cured net conductor cross-section with a filling factor of  $\geq 0.76$ . As shown in the analysis, for a more detailed finite-element model this dominating stress component in the tensor may increase. Anyway, the equivalent stress applied on the wires is less than the measured fatigue time strength for the impregnated copper wires (fig. 12) and considerably less than the hoop stresses applied to the prototype coil. Thus, under all boundary conditions described hitherto (worst-case analysis), the safety margin is above 1. Mechanically, the copper wires are not endangered.

The basis for a mechanical evaluation of the insulation system is the result obtained from the refined FE analysis. Out-of-plane direct compressive stresses, analysed up to 60 MPa, will not mechanically cause fatigue fracture of the system.

Furthermore the comparison of calculated stresses and experimental strength values are worst-case considerations, because:

- The maximum temperature rise under steady-state conditions of the coils is less than 55 K [5]. Approximately 30% of the stresses occurring in the nonplanar field coils are directly dependent on the temperature rise; see Section 2.2. Thus, the applied stresses are lower than the calculated values.
- The maximum temperature is less than 80 °C. This is also due to the reduced temperature rise within the coils and a reduced cooling water temperature under usual working conditions. Because of the heavily temperature-dependent material properties of the resin-impregnated compound material this temperature restriction will considerably raise the available (especially shear) strength values.
- The in-plane shear strength and the out-of-plane tensile strength for insulation planes perpendicular to the winding insulation are increased. This is due to the surface and winding insulation, which is analysed perpendicularly to the endangered breaking planes of the insulation system (fig. 2a).
- Only a part of the  $5 \times 10^4$  pulses envisaged during the lifetime of this machine will be full power load cycles. Thus, in comparison with the above values, the fatigue strength values – given for  $5 \times 10^4$  full load cycles at 80 °C – are increased, whereas the applied stresses – given for maximum magnetic field and a temperature rise inside the coil for steady-state conditions of 55 K – are decreased.

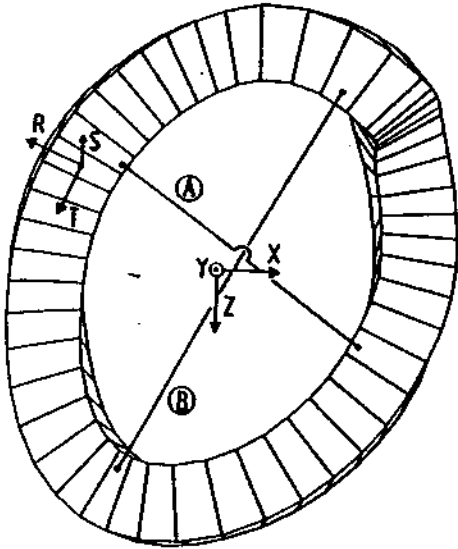
If necessary for special reasons, the available strength values and/or applied mechanical stresses may be further adapted by, for example such suitable conditions as extension of the pulse intervals or by working with the lowest possible cooling water temperature.

Finally, in a combined experimental and theoretical consideration, the assumptions, approximations, transformations and simplifications necessary to describe the behaviour of these nonplanar coils are rechecked. Especially the validity and accuracy of the mechanical and electromagnetic finite-element programs, of the calculated time-dependent thermal behaviour in the coil bulk, and of the assured material behaviour of the heterogeneous orthotropic composite material were verified. A prototype coil (shape as coil number 3 of the W VII-AS field coils) was therefore loaded by different electromagnetic forces in its self-field. The experimental tests were carried out without constraining the deformation of the prototype coil by means of the support structure, so that the effects of interaction of the nonplanar coils with other structural parts of the machine did not have



Table 2

Comparison of measured and calculated coil diameter deformation under magnetic loads, resulting from a prototype coil test in its magnetic self-field (coil number 3, side I)



$\Delta t$ (mm)		measurement	FE-analysis
minor diameter (A)	side I	1,8	2,0
	side II	1,9	2,2
major diameter (B)	side I	0,75	0,85
	side II	0,5	0,62

to be considered. The test procedure, the calculations and the measurements as well as an analysis of all the records obtained are described in detail [5,13,14,16] and may be summarised as follows:

- The measured electromechanically induced deformation in the quasilinear range of material behaviour at nominal current are compared for two diameters of the prototype coil with calculated values and show good agreement (table 2). The analysis carried out and the models used rested on the same basic foundations as for the non-sophisticated case of mechanically supported coils in a spatial arrangement with other magnets as described in Section 2.2.
- The measured temperature rise per duty cycle of the coil is lower than that predicted from conservative evaluations made by FE calculations [5]. But the calculated maximum temperature rise of 55 K was used as a basis for all calculations described in section 2.2.
- When the magnetic force is raised up to the onset of measurable material nonlinearities this onset shows good agreement with that predicted. The theoretical

magnetic force for plastic yielding was predicted by comparing analysed local stress tensors – judged by the strength hypothesis already described – as a function of the applied loads (electric current flow) with the fatigue strength values described in Sections 2.3.2 and 2.3.3.

In these tests, carried out with a prototype coil, the comparison of measured data with predicted data resulting from calculations, material tests and the interpretation show good agreement. It therefore seems admissible to transfer this knowledge to the W VII-AS field coils.

### 3. Vacuum vessel

#### 3.1. Design and construction of the vacuum vessel

A view of one modular section of the vacuum vessel is shown in fig. 17(a). It shows a test piece of original size undergoing the same manufacturing processes as envisaged for the W VII-AS vacuum vessel.

The design criteria for the vacuum vessel were as follows [e.g. 26, 27, 28, 29]:

- maximum distance between the plasma and inner vessel wall,

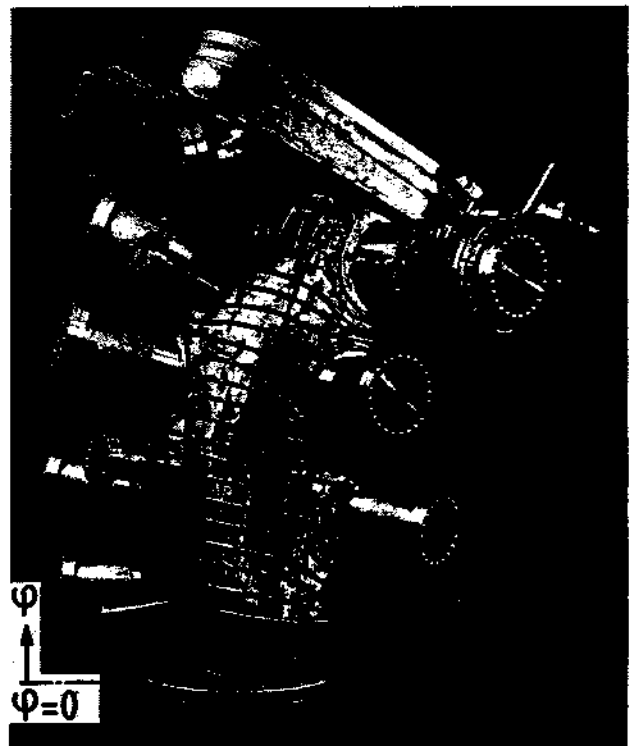


Fig. 17. The toroidal vacuum chamber: (a) test piece of a 1/10 section of the vessel, including a connection flange.

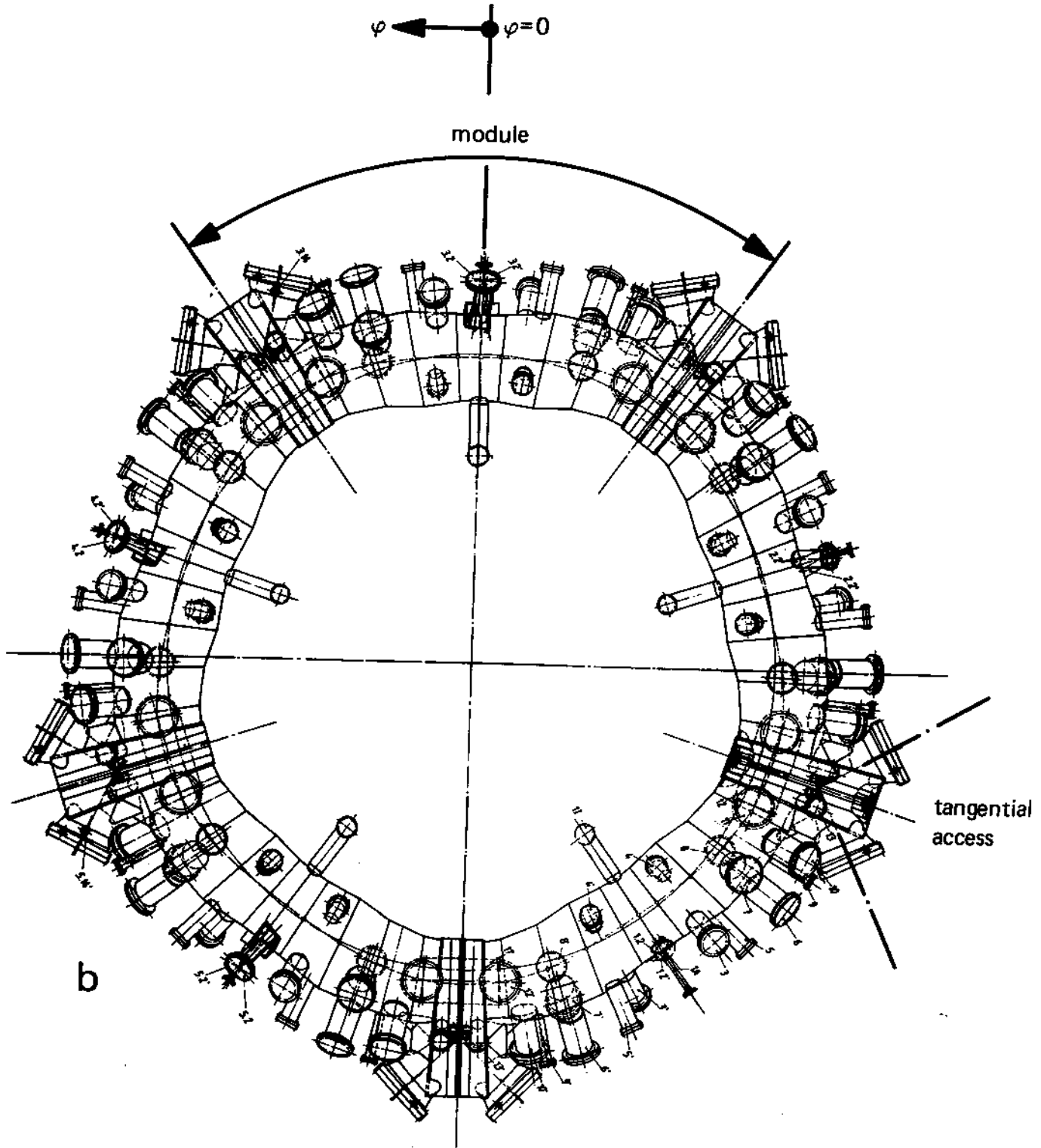


Fig. 17. The toroidal vacuum chamber: (b) plan view of the vessel, including all ports.

- minimum distance between the outer vessel wall and the MF-coils with a sufficient gap to allow radial expansion of the vessel when it is heated up, and with sufficient intermediate space for assembly,
- modularity,
- the number, size, and position of the portholes must meet the experimental requirements

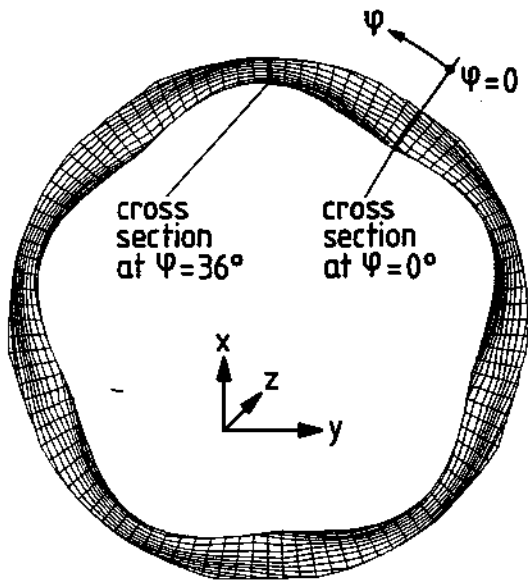


Fig. 18. Plasma column of the experiment.

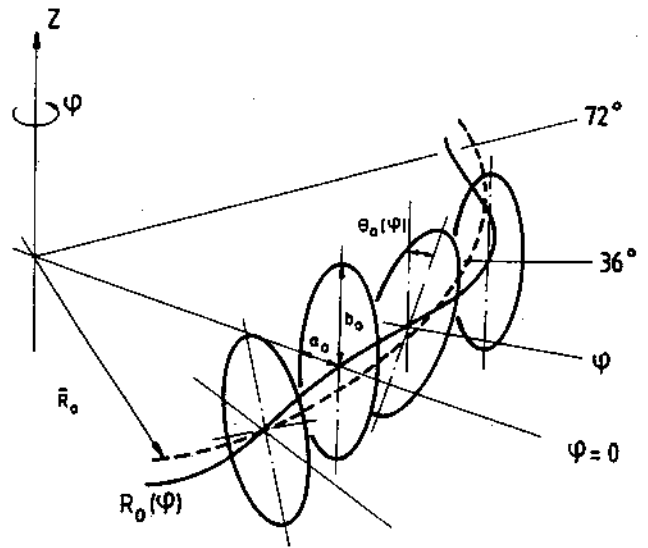


Fig. 19. Toroidal geometry of the vacuum chamber (theoretical envelope of the vacuum vessel):

$$R_0(\phi) = 2000(1.02 - 0.03 \cos 5\phi) \text{ mm},$$

$$\theta_0(\phi) = -22.5(\sin 5\phi + 0.5 \sin 10\phi) \text{ degrees}.$$

ference between this actual contour and the theoretical envelope is less than 5 mm. After being formed, each segment is individually fitted and then welded in the  $\phi$ -direction. The segments can be welded together (in the  $\theta$ -direction) into submodules, all the seams being welded through. The forming of one module of the

– simplicity of the vessel geometry to limit manufacturing costs.

In fig. 17(b) the plan view of the final design of the vessel is shown. Figure 18 shows the plasma column of W VII-AS with a cross-section varying from a triangular shape at  $\phi = 0^\circ$  to a vertical elliptical shape at  $\phi = 36^\circ$ . The cross-section of the vacuum vessel should closely match the inner bore of the MF-coils. The geometry was therefore derived from the surface current distribution [2,3,8,28] and is an approximation with

$$R_0(\phi) = 2000(1.02 - 0.03 \cos 5\phi) \text{ mm},$$

$$\theta_0(\phi) = -\pi/8 \cdot (\sin 5\phi + 0.5 \sin 10\phi),$$

to the ellipse oscillating around the magnetic axis in the  $\phi$ -direction (fig. 19). As described in the next section, a wall thickness of 12 mm was found to be sufficient. In accordance with the 5 field periods of the experiment, the vessel is divided toroidally into 5 modular sections. The volume of the vessel is approximately 7 m<sup>3</sup>. Twenty-eight ports in each module allow abundance access to the plasma for heating and diagnostics.

The two oval-shaped special ports of a module allow nearly tangential access primarily for neutral beam injection.

For reasons of economic manufacturing, the shape of the torus surface in the toroidal and poloidal direction was approximated by polygons. The toroidal polygon divides the modules into segments. These segments are formed from plane plates on a hydraulic press. The intricately curved shape of a segment is formed by appropriate bending of sheet steel (fig. 20). The dif-

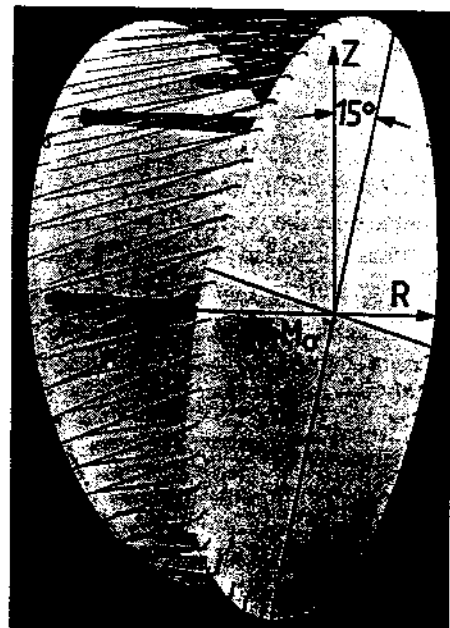


Fig. 20. Approximating the theoretical ellipse cross-section of the vacuum vessel by a polygon geometry resulting from an unroll process.

vacuum vessel is only possible after completion of the assembly of all parts of the magnetic confinement system, consisting of the MF-coils, support elements, and structure and the vessel submodules. The vacuum submodules are then welded together (seams only half-welded through to make repeated assembly possible) and finally all parts are welded into the module.

The overall construction thickness of the vessel after assembly is 20 mm. The vessel itself is a thin-walled type 304 LN stainless-steel torus, the steel wall thickness being 12 mm. The rest of the overall height is used for a pressurised hot water heating system combined with a thermal insulation system. This is necessary to produce clean vacuum conditions. To outgas the vacuum surfaces, the torus can be heated up to 150 °C by means of this system (glow discharge cleaning is envisaged to control light impurities). The thermostated water for baking the vessel circulates in copper pipes fastened to the outer torus surface. Good heat conduction to the torus is ensured by a special cement which fills the spacings between the pipes and the surface of the torus. Finally, the torus and piping system are covered by thermal insulation material (3 mm thick) to prevent excessive heat transfer to the modular field coils. All welded joints of the stainless torus are kept accessible to facilitate leak testing. When the torus is baked to 150 °C, the resulting thermal expansion is 12 mm in diameter. The rise time for the baking temperature is selected to be more than 6 h so that material stresses due to non uniform temperature fields are negligible. To prevent the deposition of unduly high heat flux from the plasma to the torus wall limiters are arranged inside the vessel.

Since a stellarator experiment does not involve induction of electric current flow in the plasma itself, the bellows necessary for tokamaks are not needed. Electrical insulation of the torus in the toroidal direction is provided in the separation planes of the 5 modules by enamel-coated sealing flanges. Vacuum sealing in the separation plane is made by helicoflex metal seals.

### 3.2. Stress analysis - Vacuum vessel

The vacuum vessel of W VII-AS is primarily subjected to gravity, vacuum, electromagnetic and thermal loads. Electromagnetic forces in a current-free stellarator, such as W VII-AS, act in the toroidal direction of the vessel during energising and de-energising of the coil system, whereas in the toroidal direction no electric current flow is induced. These electromagnetic forces - distributed over the torus surface - were calculated analytically and found to be less than  $2.5 \times 10^4 \text{ N/m}^2$

(fig. 21). A finite-element structural analysis in the final version carried out by the SULZER Comp. (manufacturers of the vessel) was made for static load conditions with the ANSYS code. The stress analyses were carried out for the following combined load case: (a) atmospheric pressure 1 bar; (b) net weight force of the vacuum vessel, which is 4.3 kN for a 1/10 section of the vessel; (c) weight force of auxiliaries limited to 30% of the vessel net weight force and distributed uniformly above the vessel (d) electromagnetic forces. The most critical loading condition occurs during de-energising of the coil system, with an electromagnetic (pressure) force of  $0.25 \times 10^5 \text{ N/m}^2$  (a very low-frequency fatigue load) superposed on the load combination mentioned above. Owing to the modularity of the test device, combined with the given load and geometry symmetries, a stress analysis for just a 1/10 section of the vessel was made. For economic reasons, this was a simplified model taking into account only the large, oval-shaped outside port (fig. 22). The influence of the smaller ports was estimated by making the conservative assumption that the effects of additional ports, acting as stiffeners for the torus and thus reducing bending stresses, were neglected. On the other hand, the weakening influence of the diagnostic ports for the membrane stresses was taken into account. The structure of the vessel for the final ANSYS stress analysis was discretized by means of 506 isoparametric triangular and quadrilateral thin shell elements (522 nodes). They include both membrane and bending stiffness. For type 304 LN (X2CrNiN1810) stainless steel the material data are as follows: Young's modulus  $2 \times 10^5 \text{ MPa}$ , yield strength 260 MPa (20 °C) and 180 MPa ( $\approx 150 \text{ °C}$ ), isotropic material behaviour.

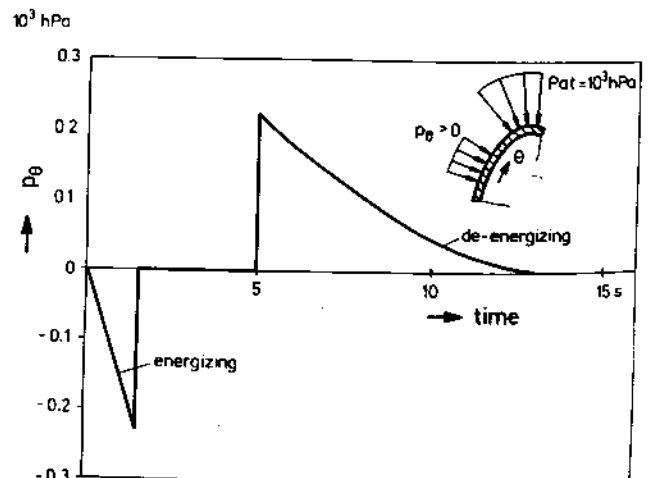


Fig. 21. Electromagnetic load on the vacuum chamber during energising and de-energising of the coil systems (vacuum field on torus axis max. 3.5 T).

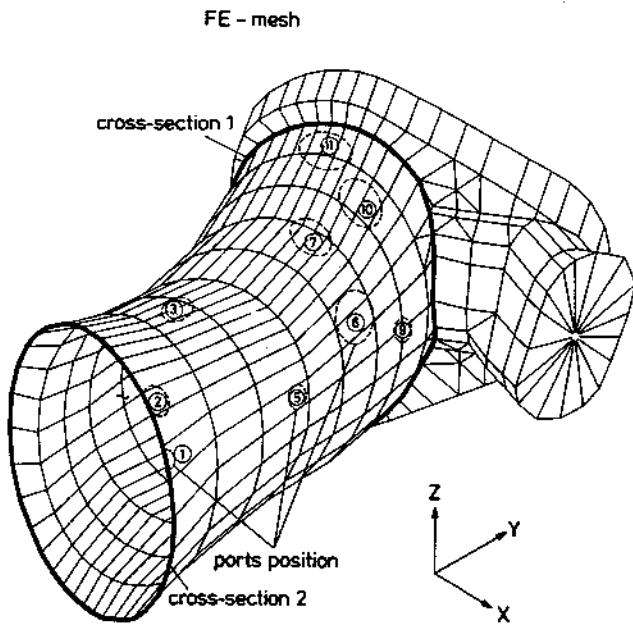


Fig. 22. FE structural model for the stress analysis of a 1/10 section of the toroidal vacuum chamber (for the cross-sections marked see fig. 23).

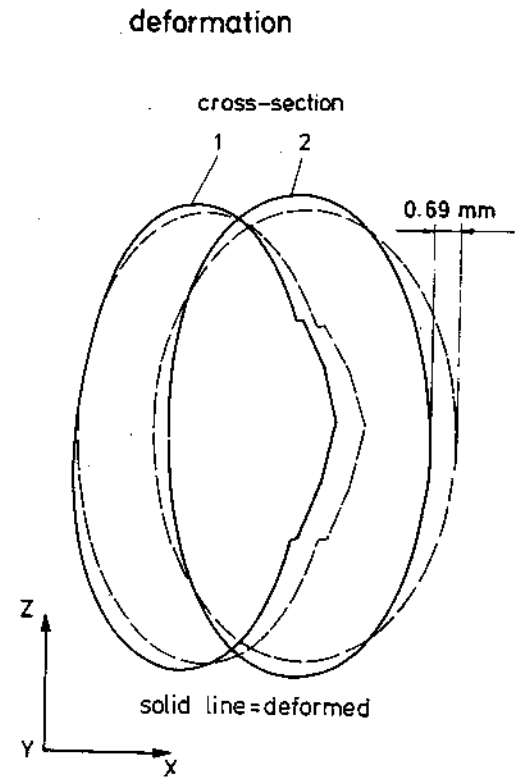


Fig. 23. Deflected and undeflected forms of two cross-sections of the toroidal vacuum chamber (scaling factor 100, only vacuum and electromagnetic loads).

Figure 23 shows the deformation of the vacuum vessel in cross-section. These deformations are small compared with the thermal expansion induced by heating the torus to 150 °C (< 6 mm maximum one side). The clearance between the torus and the MF-coils of more than 10 mm everywhere is thus sufficient with respect to the calculated displacement induced by combined magnetic, vacuum and gravity loads as well as those induced by unrestrained thermal expansion. The maximum displacement of 0.8 mm appears at the symmetry plane of the vessel model (fig. 23).

As derived from corresponding ASTM (American Society for Testing and Materials) regulations and AD specifications (German Arbeitsgemeinschaft Druckbehälter Merkblätter [30]), the safe working stresses for austenitic (stainless) steels must be below the following limits: (a) for membrane stresses  $\sigma_m < S_M = R_{p,0.2} / 1.1 = 164 \text{ MPa}$  (type 304 LN, 150 °C); (b) for linear stresses (membrane and bending)  $\sigma_{m+b} < 1.5 S_M = 245 \text{ MPa}$ .

The maximum equivalent (Von Mises) stresses obtained from the static structural analysis with the FE model described above are  $\sigma_{eq}^m$  (membrane) = 42.5 MPa and  $\sigma_{eq}^{m+b}$  (membrane + bending) = 84.6 MPa (table 3), localized in the transition region near the insulation flange of the module/torus. For only half welded through seams in the torus shell of the vessel the stresses were estimated on the basis of the FE calculations. The membrane stress component of the equivalent stress for half wall thickness is double the value obtained from

the FE analysis, and the linear component is 4 times the value obtained from the analysis for  $\sigma_{eq}^{m+b}$ . The calculated maximum stress intensities for half welded through seams are  $\sigma_{eq}^m = 76.8 \text{ MPa}$  and  $\sigma_{eq}^{m+b} = 228 \text{ MPa}$  (table 3).

When comparing safe working stress limits with those stress values obtained from the FE analysis or derived from these results by adequate evaluations, one can see

Table 3

V. Mises stresses (membrane and bending component) in the toroidal vacuum chamber as obtained from the simplified FE analysis and estimated on this basis with allowance for ports and welded seams

v. Mises stresses [MPa]	maximum value obtained from FE-analysis	estimated value for half-welded through seams	web between port 10 and 11		safe working limit s
			obtained from FE-analysis	considering weakening influence	
$\sigma_{eq}^m$	42,5	76,8	15,0	47,2	164
$\sigma_{eq}^{m+b}$	84,6	228,0	35,5	67,7	245

that the stresses determined are within the allowable levels for static loads (table 3). The safe working stresses are not heavily influenced (decreased) by fatigue loads resulting from the electromagnetic pulsed load. This is because this load component is comparatively small and the fatigue strength of austenitic steel decreases only slightly from static (0.2% proof) strength values (especially for the lifetime of the machine envisaged,  $5 \times 10^4$  load cycles). The W VII-AS vacuum vessel will thus be capable of withstanding the loads applied, even under fatigue loads. The critical buckling load of the (thick-walled) stainless-steel vacuum vessel, estimated by using the regulations given in [30] and formulas given in [31], is many times higher than the actual (primary vacuum) load.

#### 4. Status of the experiment

##### 4.1. First experimental results

The confinement system of the device, including the vacuum vessel, was assembled in early spring 1988 (fig.

24). Magnetic field mapping, succeeded in May and June 1988, first plasma operation of the experiment in Oct. 1988.

The evaluation of the field mapping experiments showed that in the W VII-AS Stellarator it has been demonstrated by means of modular field coils that it is possible to produce magnetic surfaces which are in very good agreement with the numerical predictions.

Also the first thousands of plasma discharges – preferably heated with radio frequency power at the electron resonance frequency of 70 GHz and with some hundred kilowatts – showed expected performance. Experiments with enlarged heating power are planned, as well as the use of additional heating methods like neutral beam injection and ion cyclotron resonance heating. A mechanical problem appeared with one type of the small non-planar coils (No. 3) in the coil set: the displacements at nominal load are much higher than predicted in the FE-calculation and acting in other directions. Therefore it has to be assumed that the stress distribution and combination discussed earlier in that paper are not representative for that coil. To prevent predamaging of the insulation the allowed magnetic

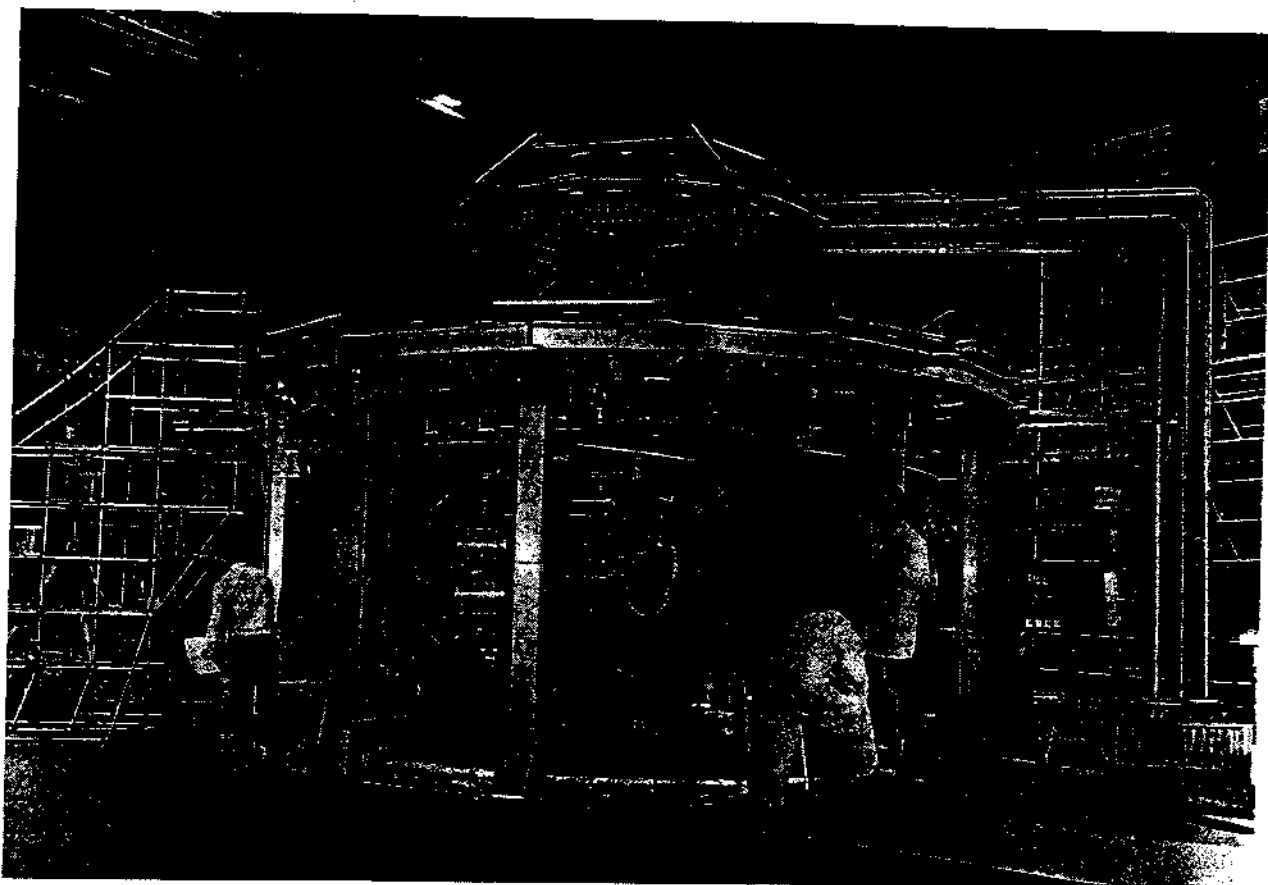


Fig. 24. Total view of the WENDELSTEIN VII-AS experimental device, status May 1988.

fields in the machine were limited to approx. 60% of nominal values. Investigations for detailed analysis are on the way and will be reported in a further publication after final evaluation.

### Acknowledgements

Thanks for contributions to and support of this work are due to the W VII-AS project and design team of our institute (W. Bitter, U. Brossmann, D. Dorst, H. Gillhuber, A. Hasenmüller, E. Harmeyer, S. Huber, E. Katzmarek, F. Kerl, J. Kisslinger, T. von Larcher, W. Melchior, H. Münch, S.B. Mukherjee, H. Renner, I. Schoenewolf, B. Sombach and H. Wobig) and to our main contractors: BBC Company, Mannheim, F.R.G. (K.E. Buck, K.D. Huber and D. Klee), SULZER Company, Winterthur, Switzerland (R. Brook) and IABG Company, Ottobrunn, F.R.G. (G. Gröger and R. Schäfer).

### References

- [1] H. Wobig and S. Rehker, A Stellarator coil system without helical windings, Proc. of the VII SOFT, Grenoble, 1972, p. 345.
- [2] J. Kisslinger, F. Rau and H. Wobig, Vacuum magnetic fields and modular coil system of the Wendelstein VII-AS advanced stellarator, Proc. 12th Symp. on Fusion Technology, Jülich (Pergamon Press, Oxford, 1982) pp. 1051–1057.
- [3] K.E. Buck and J.W. Hammel, Fabrication effects on the structural behaviour of large coils for fusion experiments, Nucl. Engrg. Des. 54 (1979) 225–238.
- [4] K.D. Huber, Modular coils for the Wendelstein VII-AS plasma experiment, Brown Boveri Review 74 (1987) 75–77.
- [5] R. Mathis and J. Sapper, Comparison of measured and calculated behaviour of Wendelstein VII-AS components – First results, Trans. of the 9th Int. Conf. on Structural Mechanics in Reactor Technology, Lausanne, Switzerland (Balkema Publishers, Rotterdam, 1987) Part N, pp. 25–30.
- [6] U. Brossmann, F. Kerl, W. Melchior, S. Mukherjee, J. Sapper and B. Sombach, Modular design of the W VII-AS advanced stellarator – Engineering details, Proc. of the 10th Symp. on Fusion Engineering, Philadelphia, USA, IEEE (1983) pp. 1569–1572.
- [7] S.I. Sackett, EFFI – a code for calculating the electromagnetic field, force and inductance in coil systems for arbitrary geometry, Lawrence Livermore Laboratory, Report UCRL-52402 (1978).
- [8] U. Brossmann, S. Mukherjee and J. Sapper, Mechanical stress analysis for the twisted coils of the Wendelstein VII-AS advanced stellarator, Proc. of the 12th Symp. on Fusion Technology, Jülich, FRG (Pergamon Press, Oxford, 1982) pp. 991–996.
- [9] R. Mathis, S.B. Mukherjee and J. Sapper, Mechanical analysis and material tests of the twisted Wendelstein VII-AS coils, Proc. of the 8th Int. Conf. on Structural Mechanics in Reactor Technology, Brussels, Belgium (North-Holland, Amsterdam, Physics, 1985) Part N, pp. 23–29.
- [10] C.W. McCormick, MSC/NASTRAN User's Manual, MacNeal-Schwendler Corp., Los Angeles, CA MSR 39 (1978).
- [11] R. Mathis and J. Sapper, Application of finite-element methods to the design of a torus-shaped magnetic confinement system for fusion experiments, Int., Conf. on Computational Techniques and Applications 1987, Sydney, Australia, CTAC 1987 (North-Holland, Amsterdam, 1988) pp. 461–474.
- [12] R. Mathis, Arbeitsbericht Projekt W VII-AS, Max-Planck-Institut für Plasmaphysik (1986).
- [13] K.E. Buck, O. Osen, U. von Bodisco and K. Winkler, Structural analysis of large magnetic coils, Proc. Finite Elements in Engineering Application, Stuttgart (1987) pp. 173–192.
- [14] K.E. Buck, P. Klee and R. Mathis, Festigkeitsnachweis für die großen Spulen des Plasmaexperimentes Wendelstein VII-AS, ABB-Technik, Heft 2 (1989) 17–24.
- [15] Schrem et al., ASKA User's Ref. Manual, Rev. F, ISD-Report 73, Univ. Stuttgart (1979).
- [16] R. Mathis and J. Sapper, Structural analysis of magnet coils, Proc. of the 3rd Int. Conf. on Computational Methods and Experimental Measurement, Porto Caras, Greece (Springer Verlag, Berlin, Heidelberg, 1986) pp. 229–249.
- [17] J. Sapper, U. Brossmann, G. Grieger, J. Kisslinger, S. Mukherjee, F. Rau, B. Sombach and H. Wobig, The WENDELSTEIN VII-AS advanced stellarator, 12th Symp. on Fusion Technology, Jülich, FRG (Pergamon Press, Oxford, 1982) pp. 161–166.
- [18] R. Mathis, J. Sapper and I. Schoenewolf, Engineering problems of the Wendelstein VII-AS experiment, Proc. of the 8th Int. Conf. on Structural Mechanics in Reactor Technology, Brussels, Belgium (North-Holland, Amsterdam, 1985) pp. 15–21.
- [19] A.A. Koch, R.K. Maix and K. Nylund, Insulation systems for magnets used in experiments for nuclear fusion and high-energy research, Brown Boveri Review 65, No. 5 (1978) 326–333.
- [20] J.C. Rauch, F. König and T. Schmid, Test program on the insulation system for the JET inner poloidal coils, Trans. 11th Symp. Fusion Technology (Pergamon Press, Oxford, 1980) pp. 449–454.
- [21] J.R. Last, A. Bond and E. Salpietro, Mechanical tests on insulation systems for the JET poloidal coils, Proc. of the 10th Symp. on Fusion Technology, Padova, Italy (Pergamon Press, Oxford, 1978) pp. 1025–1031.
- [22] S.W. Tsai and E.M. Wu, A general theory of strength for anisotropic materials, J. of Composite Materials 5 (1970) 58–80.

- [23] A. Puck and H. Schürmann, Die Zug/Druck-Torsionsprüfung and rohrförmigen Probekörpern, *Kunststoffe* 72 (1982) 554–561.
- [24] R. Bandenheier, Mechanisches Versagen von Kunststoffen – Anstrengungsbewertung mehraxialer Spannungszustände, *Kunststoffe* 72 (1982) 729–732.
- [25] W. Knappe and W. Schneider, Bruchkriterien für unidirektionalen Glasfaser/Kunststoff unter ebener Kurzzeit- und Langzeitbeanspruchung, *Kunststoffe* 62 (1982) 864–868.
- [26] D. Dorst, G. Grieger, R. Mathis and J. Sapper, The Wendelstein VII-AS experiment, *Proc. of the 14th Symp. on Fusion Technology*, Avignon, France (Pergamon Press, Oxford, 1986) Part 1, pp. 139–148.
- [27] J. Sapper, U. Brossmann, G. Grieger and H. Wobig, Modular design of the W VII-AS advanced stellarator – Overview, *Proceedings 10th Symp. on Fusion Engineering*, IEEE, Philadelphia, USA, 1983, Paper 6 D 01.
- [28] See ref. [6].
- [29] R. Rau, J. Kisslinger, and H. Wobig, Vacuum magnetic field and modular coil system of the WENDELSTEIN VII-AS advanced stellarator, IPP Report 2/259 (1982).
- [30] AD-Merkblatt B6, Berechnung von Druckbehältern, TÜV, FRG (1977).
- [31] R.J. Roark and W.C. Young, *Formulas for Stress and Strain* (McGraw-Hill, New York, 5th edition, 1975).